



HAL
open science

Assessing anoxia, recovery and carbonate production setback in a hemipelagic Tethyan basin during the Toarcian Oceanic Anoxic Event (Western Carpathians)

Tamás Müller, Szabina Karancz, Emanuela Mattioli, Rastislav Milovský, József Pálffy, Jan Schlögl, Tomasz Segit, Vladimír Šimo, Adam Tomašových

► To cite this version:

Tamás Müller, Szabina Karancz, Emanuela Mattioli, Rastislav Milovský, József Pálffy, et al.. Assessing anoxia, recovery and carbonate production setback in a hemipelagic Tethyan basin during the Toarcian Oceanic Anoxic Event (Western Carpathians). *Global and Planetary Change*, 2020, 195, 10.1016/j.gloplacha.2020.103366 . insu-03710126

HAL Id: insu-03710126

<https://insu.hal.science/insu-03710126v1>

Submitted on 30 Jun 2022

HAL is a multi-disciplinary open access archive for the deposit and dissemination of scientific research documents, whether they are published or not. The documents may come from teaching and research institutions in France or abroad, or from public or private research centers.

L'archive ouverte pluridisciplinaire **HAL**, est destinée au dépôt et à la diffusion de documents scientifiques de niveau recherche, publiés ou non, émanant des établissements d'enseignement et de recherche français ou étrangers, des laboratoires publics ou privés.



Distributed under a Creative Commons Attribution 4.0 International License



Research article

Assessing anoxia, recovery and carbonate production setback in a hemipelagic Tethyan basin during the Toarcian Oceanic Anoxic Event (Western Carpathians)

Tamás Müller^{a,b,*}, Szabina Karancz^{c,d}, Emanuela Mattioli^{e,f}, Rastislav Milovský^a, József Pálffy^{g,h}, Jan Schlöglⁱ, Tomasz Segit^j, Vladimír Šimo^a, Adam Tomašových^a

^a Earth Science Institute, Slovak Academy of Sciences, Dúbravská cesta 9, 84005 Bratislava, Slovakia

^b Isotope Climatology and Environmental Research Centre, Institute for Nuclear Research, Bem tér 18/C, H-4026 Debrecen, Hungary

^c Department of Ocean Systems, Royal Netherlands Institute for Sea Research (NIOZ), Landsdiep 4, 1797 SZ 't Horntje, Texel, the Netherlands

^d Department of Earth Sciences, Faculty of Geosciences, Utrecht University, Princetonaan 8A, 3584, CB, Utrecht, the Netherlands

^e ENSL, CNRS, LGL-TPE, Univ Lyon1, Univ Lyon, F-69622 Villeurbanne, France

^f Institut Universitaire de France (IUF), France

^g Department of Geology, Eötvös Loránd University, Pázmány Péter sétány 1/C, Budapest H-1117, Hungary

^h MTA-MTM-ELTE Research Group for Paleontology, POB 137, H-1431 Budapest, Hungary

ⁱ Department of Geology and Paleontology, Faculty of Natural Sciences, Comenius University in Bratislava, Mlynská dolina-G, Ilkovičova 6, Bratislava 842 15, Slovakia

^j Institute of Geology, University of Warsaw, Żwirki i Wigury 93, Warszawa 02-089, Poland

ARTICLE INFO

Keywords:

Toarcian OAE
Calification crisis
Carbon isotope stratigraphy
Tethyan margin
Bioturbation

ABSTRACT

The chemostratigraphic record of the Toarcian Oceanic Anoxic Event (T-OAE) is generally well documented in epicontinental basins; however, the duration of anoxia and recovery remains poorly constrained in the Tethys Ocean owing to limited stratigraphic resolution of oceanic sections with hiatuses. In this paper, we describe a relatively continuous hemipelagic record in the Central Western Carpathians of Slovakia (Skladaná Skala section), which contains the Pliensbachian/Toarcian boundary, the T-OAE, and the subsequent recovery phase. In our section, the Pliensbachian Spinatum Zone is represented by a ~7 m thick alternation of spotted, spiculitic marly limestones and limestones of the Allgäu Formation that contain moderately diverse trace fossils including abundant *Zoophycos*, *Lamellaichnus* and *Teichichnus*. In the uppermost part of the Spinatum Zone, a ~0.8‰ decline in $\delta^{13}\text{C}_{\text{carb}}$ values marks the carbon isotope excursion (CIE) at the Pliensbachian/Toarcian boundary. This isotope anomaly is overlain by a ~3 m-thick interval of spotted marly limestones and marls, which contains a positive CIE that represents the base of the T-OAE. The T-OAE interval comprises a 60 cm-thick pyritic black shale interval that lacks bioturbation and shows a negative CIE ($\delta^{13}\text{C}_{\text{org}}$ values drop by 4–5‰), coincident with an increase in TOC values (from 0.3% to 2–3%), and a drop in CaCO_3 values (from 50 to 80% to 3–7%). The black shale is overlain by ~8 m thick marls with rare intercalations of marly limestones, which show ammonites of the Exaratum Subzone in the lowermost part (~1 m) succeeded by Serpentinum Zone beds. This unit exhibits a second positive CIE ($\delta^{13}\text{C}_{\text{org}}$ increases by 2.5‰ and $\delta^{13}\text{C}_{\text{carb}}$ increases by 1.5‰), significantly more negative $\delta^{18}\text{O}$ values relative to the pre-T-OAE interval, and a low diversity of trace fossils dominated by *Chondrites* and extremely thin *Zoophycos*. Sponge spicules re-appear in the uppermost 6.5 m-thick interval of the section formed by the alternation of spotted marls and limestones, with ammonites of the Falciferum Subzone in the lower part and of the Bifrons Zone in the uppermost parts; however, diversity of trace fossils remains low. Based on these findings, we argue that the 60 cm-thick pyritic black shale that represents the T-OAE is a strongly condensed succession because it includes the onset of the negative CIE and the subsequent rebound, and thereby encompasses the full duration of the anoxic event. Anoxia in basins open to the oceanic Tethys thus coincided not only with reduced carbonate production but also with reduced siliciclastic supply, generating very thin black shale deposits. In contrast to current-swept swells where black shales associated with hardgrounds are thin or missing owing to winnowing, carbonate starvation was induced by a calcification crisis coincident with the T-OAE and siliciclastic starvation was probably induced by rapid sea-level rise. Although bottom waters were not anoxic in

* Corresponding author at: Earth Science Institute, Slovak Academy of Sciences, Dúbravská cesta 9, 84005 Bratislava, Slovakia.

E-mail address: beregond02@gmail.com (T. Müller).

<https://doi.org/10.1016/j.gloplacha.2020.103366>

Received 20 November 2019; Received in revised form 27 October 2020; Accepted 27 October 2020

Available online 2 November 2020

0921-8181/© 2020 The Authors. Published by Elsevier B.V. This is an open access article under the CC BY license (<http://creativecommons.org/licenses/by/4.0/>).

the aftermath of T-OAE, bioturbation remained restricted during the Falciferum Subzone in basinal settings, indicating that environmental stress induced by limited ventilation and/or high bottom-water temperatures were persistent. The reduced diversity of trace fossils and the re-appearance of sponge spicules close to the lower/middle Toarcian boundary indicate that the ecological recovery in basins open to the oceanic Tethys was delayed, a pattern similar to the epicontinental seas that experienced anoxia.

1. Introduction

Two major carbon cycle perturbations related to CO₂ emissions from the Karoo-Ferrar large igneous province and/or thermal metamorphism of coal sediments in the Karoo Basin (e.g. McElwain et al., 2005; Svensen et al., 2007) are detected at the Pliensbachian-Toarcian boundary (Pl-To) (Littler et al., 2010) and during the Toarcian Oceanic Anoxic Event (T-OAE, Jenkyns, 1988; Jenkyns Event in Müller et al., 2017). These anomalies were associated with a second order mass extinction and faunal turnover in the composition of benthic and pelagic ecosystems, anoxia, global warming, and ocean acidification (Pálffy and Smith, 2000; Macchioni and Cecca, 2002; Bailey et al., 2003; Hesselbo et al., 2007; Caswell et al., 2009; Mattioli et al., 2009; Suan et al., 2010; Trecalli et al., 2012; Reolid et al., 2012a, 2012b; Müller et al., 2020). It has been also observed that the global extent of anoxia during the T-OAE led to widespread burial of organic carbon and consequently to deposition of organic-rich black shales in both marine and lacustrine settings (Wignall et al., 2005; Xu et al., 2017; Suan et al., 2018). The carbon cycle perturbations are expressed by a short-term negative carbon isotope excursion (CIE) at the Pl-To (Hesselbo et al., 2007; Littler et al., 2010; Bodin et al., 2016), followed by a broad positive excursion during the early Toarcian which was interrupted by a remarkably large (~ 5‰) negative CIE at the onset of the T-OAE (e.g. Hesselbo et al., 2007; Hermoso et al., 2012; Müller et al., 2017). This pattern has been detected both in bulk and biogenic carbonates and in marine and terrestrial organic matter around the globe (e.g. Gröcke et al., 2011; Al-Suwaidi et al., 2016; Izumi et al., 2018), but primarily in Peri-Tethyan epicontinental seas (e.g. Kemp et al., 2005; Gómez et al., 2008; Hermoso et al., 2009; Suan et al., 2008a; Hesselbo and Pieńkowski, 2011).

During the T-OAE, both the NW European epicontinental basins (Röhl et al., 2001; McArthur et al., 2008; Thibault et al., 2018) and ocean-facing Tethyan shelves bordering the NW European platform were affected by widespread anoxia (Wignall et al., 2005; Suan et al., 2018; Müller et al., 2017; Ruebsam et al., 2018). The benthic recovery was more rapid and occurred in the wake of the T-OAE during the Serpentinum Zone on shelves that were not or only weakly affected by anoxia (e.g. in the Iberian Range, in the Lusitania Basin and in the Sahara Atlas; Gahr, 2005; Reolid et al., 2012a; Miguez-Salas et al., 2017; Piazza et al., 2019). In contrast, the benthic recovery was delayed up to the onset of the next ammonite zone, i.e., it occurred during the Bifrons Zone, on epicontinental shelves that experienced long-term anoxia (García-Joral and Goy, 2009; García-Joral et al., 2011; Danise et al., 2015; Martindale and Aberhan, 2017). However, the dynamics of the T-OAE and the ecosystem recovery in deeper Tethyan oceanic environments not directly attached to the European shelf remain poorly documented or unknown. These environments were differentiated during the Pliensbachian and Toarcian into current-swept structural highs with condensed sedimentation (nodular limestones and hardgrounds) and more sheltered basins with less condensed marly hemipelagic deposits (Fig. 1). Chemostratigraphic analyses of sections proximal to oceanic domain documented high variation in the expression of the T-OAE owing to differences in water depth and sedimentation rate (Jenkyns et al., 1991; Sabatino et al., 2009; Arabas et al., 2017; Fantasia et al., 2019). Chemostratigraphic analyses across the T-OAE in Tethyan hemipelagic-pelagic basins either (1) documented long-term anoxia in the strongly restricted Úrkút and Bächtental basins (with Mn-rich sediments and unique basin-specific diagenetic conditions, Vetö et al., 1997; Neumeister et al., 2015; Polgári et al., 2016) or (2) inferred that anoxic

conditions were short-living or negligible (e.g., in the Betic Cordillera Rodríguez-Tovar and Uchman, 2010). Deeper bathyal open-oceanic environments, less sensitive to water stratification in contrast to semi-enclosed epicontinental basins, may represent refugia for benthic groups under major environmental disturbances (Smith and Stockley, 2005; Vörös, 2005; Thuy et al., 2012). For example, Baeza-Carratalá et al. (2017) suggested that a deep pelagic trough on the South-Iberian palaeomargin (External Subbetic) represented a refugium for some brachiopod lineages. However, understanding the nature and distribution of these refugia during the T-OAE remains limited as the extent and duration of anoxia and the extent of bottom-water warming (i.e., factors that affected ecosystem dynamics and extinctions of benthic fauna during the T-OAE in shelf environments; García-Joral et al., 2011; Gómez and Goy, 2011; Baeza-Carratalá, 2013; Them et al., 2018; Ullmann et al., 2020) in these deeper oceanic environments is poorly understood.

For example, on the basis of bioturbation intensity and trace fossil diversity, Rodríguez-Tovar and Uchman (2010) and Rodríguez-Tovar and Reolid (2013) suggested that the duration of bottom-water oxygen depletion was rather short and that benthic communities (with burrowers and foraminifers) recovered quickly in the aftermath of the T-OAE during the Serpentinum Zone at the Fuente Vidriera section in the Betic Cordillera. A similar pattern in the recovery of trace-fossil assemblages was observed in other hemipelagic sections in the Betic Cordillera (Reolid et al., 2014; Gallego-Torres et al., 2015). However, these findings of short-term or insignificant anoxia in hemipelagic oceanic basins and the estimates of rapid recovery can be biased by a reduced sedimentation rate during the T-OAE, and to a certain extent, by post-anoxic bioturbation (Danise et al., 2019). Both benthic and pelagic carbonate production was significantly reduced during the T-OAE (Mattioli et al., 2009; Trecalli et al., 2012; Ettinger et al., 2020; Krencker et al., 2020) and rapid sea-level rise associated with the T-OAE could induce starvation of siliciclastics in distal settings (Pittet et al., 2014). Therefore, investigations of sedimentological, paleoecological and chemostratigraphic patterns in continuous sections spanning the upper Pliensbachian-lower Toarcian are needed to assess the completeness and resolution of the T-OAE in deeper basinal settings of the Tethys Ocean. Here, we analyze the Pliensbachian-Toarcian sediments in the Central Western Carpathians and document that organic-rich laminated sediments and the Toarcian negative CIE are preserved just within ~60 cm thick condensed unit. In contrast to hemipelagic sections in the Betic Cordillera, benthic recovery was delayed throughout the Serpentinum Zone, similarly as in epicontinental seas.

2. Paleogeographic and stratigraphic setting

The Skladaná Skala section is located in an abandoned quarry on the northern margin of the Veľká Fatra Mountains of Slovakia (49°7' 15.66" N; 19°13' 27.98" E), part of the Fatric Superunit (Křížna Nappe) of the Central Western Carpathians (CWC). Paleogeographically, the CWC represents an eastern analog of the Austroalpine system during the Mesozoic. The Fatric Superunit, equivalent to the middle Austroalpine units in the Northern Calcareous Alps (Häusler et al., 1993), was bordered to the north by the shallower, more uplifted Tatric Superunit and passed to the south to the Veporic Unit (also partly equivalent to the middle Austroalpine units) and Hronic and Silicic units (equivalents to the upper Austroalpine units). During the Hettangian, the Central Western Carpathians were still attached to the passive European margin

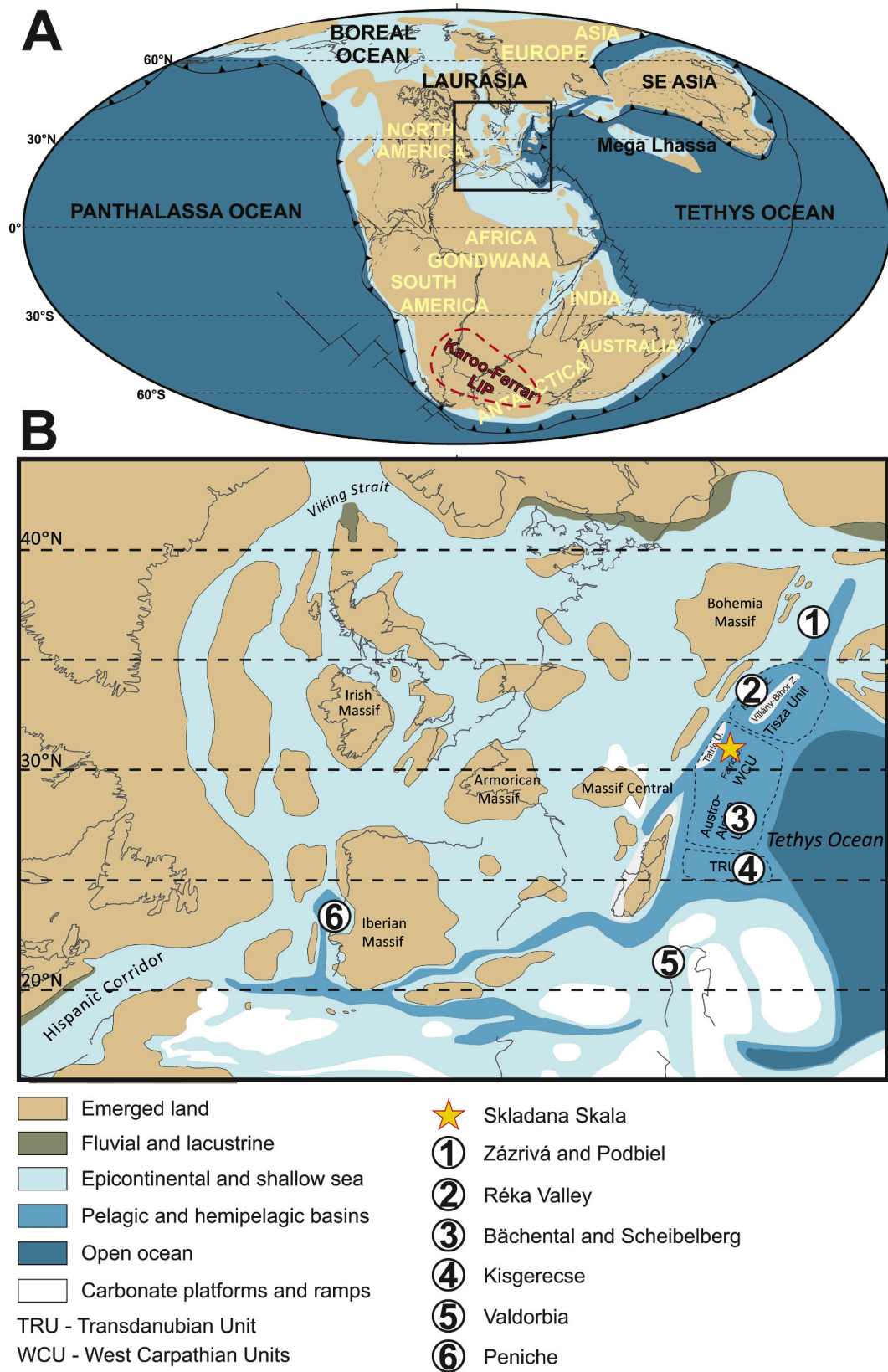


Fig. 1. A: Continent configuration and paleogeographic map of the Toarcian, indicating also the location and areal extent of the Karoo-Ferrari LIP (after [Montero-Serrano et al., 2015](#)). B: Paleogeographic map of the NW Tethys (modified from [Thierry, 2000](#)), and the positions of the NW Tethyan tectonic units (TRU: Transdanubian Unit, Austro-Alpine Units, WCU: Western Carpathian Units and Tisza Unit; supposed areas marked with dashed line). Modified from [Häusler et al. \(1993\)](#) and [Haas \(2012\)](#). Numbered sites are the ones selected for comparison and chemostratigraphic correlation (see [Fig. 9](#)).

of the NW Tethys (Fig. 1).

The Kopieniec Formation was deposited on a shallow, mixed carbonate-siliciclastic ramp during the Hettangian in most depositional environments of the Fatric Superunit. Similarly to other regions of the Alpine Tethys (Krainer et al., 1994; Krainer and Mostler, 1997; Jiménez et al., 1996), the Fatric Superunit was differentiated into swells and basins during the Sinemurian, with the deposition of crinoidal and oncoidal limestones on the shallowest swells, nodular and spiculitic limestones on swells and slopes, and spotted limestones and marls in grabens (Koša, 1998; Gradziński et al., 2004; Jach, 2005). The Sinemurian-Toarcian in basins in the Fatric Superunit are represented by spotted limestones and marls (Fleckenkalk and Fleckenmergel) of the Allgäu Formation (Rakús, 1963, 1964; Gradziński et al., 2004) (also referred to as Janovky Formation by Gaździcki et al., 1979 or as the Soltysia Marl Formation by Lefeld et al., 1985). In the southern and central parts of the Velká Fatra Mountains, this formation pinches out and is replaced by red nodular limestones of the Adnet Formation (Mišík and Rakús, 1964). Towards the north, the Allgäu Formation is also exposed in the northern parts of the Malá Fatra Mountains and in the West Tatra Mountains, where it can horizontally pass into spiculitic and crinoidal limestones, indicating proximity of another swell (Jach, 2002; Iwańczuk et al., 2013).

At Skladaná Skala, upper Sinemurian-middle Toarcian deposits of the Allgäu Formation, from the Oxynotum Zone up to the Bifrons Zone, are exposed (Rakús, 1964, 1984). Rakús (1984) subdivided the succession into three units, including the lower, ~70 m-thick unit of marly limestones that contain late Sinemurian ammonites (*Oxynotoceras oxynotum* and *Echioceras raricostatum*), the middle, ~225 m-thick unit formed by alternation of limestones and marly limestones with late Pliensbachian ammonites in its upper part (*Amaltheus stokesi* and *Pleuroceras spinatum*), and the upper, ~70 m-thick unit that is characterized by the prevalence of marls with lower and middle Toarcian ammonites. Our work is focused on the upper part of the middle unit and on the

upper unit. Šimo and Tomašových (2013) described trace fossils from the upper part of the lower unit and from the middle unit in this section.

3. Materials and methods

Two sections that were sampled at the Skladaná Skala locality expose upper Pliensbachian-lower Toarcian strata. About ~25.4 m were logged in the western part of the quarry (S1) and 3.4 m (S2) on the eastern side of the quarry (Fig. 2). The T-OAE is preserved in a segment that overlies Bed 63 and it is better exposed at S2 than at S1 where this interval is affected by tectonic dislocations (low angle normal fault) (Fig. S1), therefore S2 was chosen as a complementary section. The two sections were correlated on the basis of ammonites of the Exaratum Subzone that occur immediately above Bed 64 and chemostratigraphy (Fig. S1). The sampling interval was 10 cm for geochemical and ~30 cm for nannofossil samples. 285 samples were collected for bulk rock analyses of CaCO₃, total organic carbon content (TOC), organic carbon isotopes ($\delta^{13}\text{C}_{\text{org}}$) and carbonate carbon ($\delta^{13}\text{C}_{\text{carb}}$) and oxygen ($\delta^{18}\text{O}_{\text{carb}}$) isotopes. Samples for analyses of microfacies in thin sections and for analyses of trace-fossil assemblages in polished cross-sections were collected at regular, ~20 cm intervals.

Nannofossil assemblages were analyzed in 48 samples. The bulk sediment samples first were cleaned with a brush and then carefully sampled with a carbide pen under a binocular microscope to collect ~100 mg of micritic material, avoiding altered parts for carbonate carbon and oxygen isotope analyzes. Aliquots of the material were pulverized and homogenized (~10–60 g) in a rock mill in order to process them for organic carbon isotope, TOC and total carbonate analyzes. Stable isotope, TOC and total carbonate analyzes were performed at the Earth Science Institute of the Slovak Academy of Sciences in Banská Bystrica.

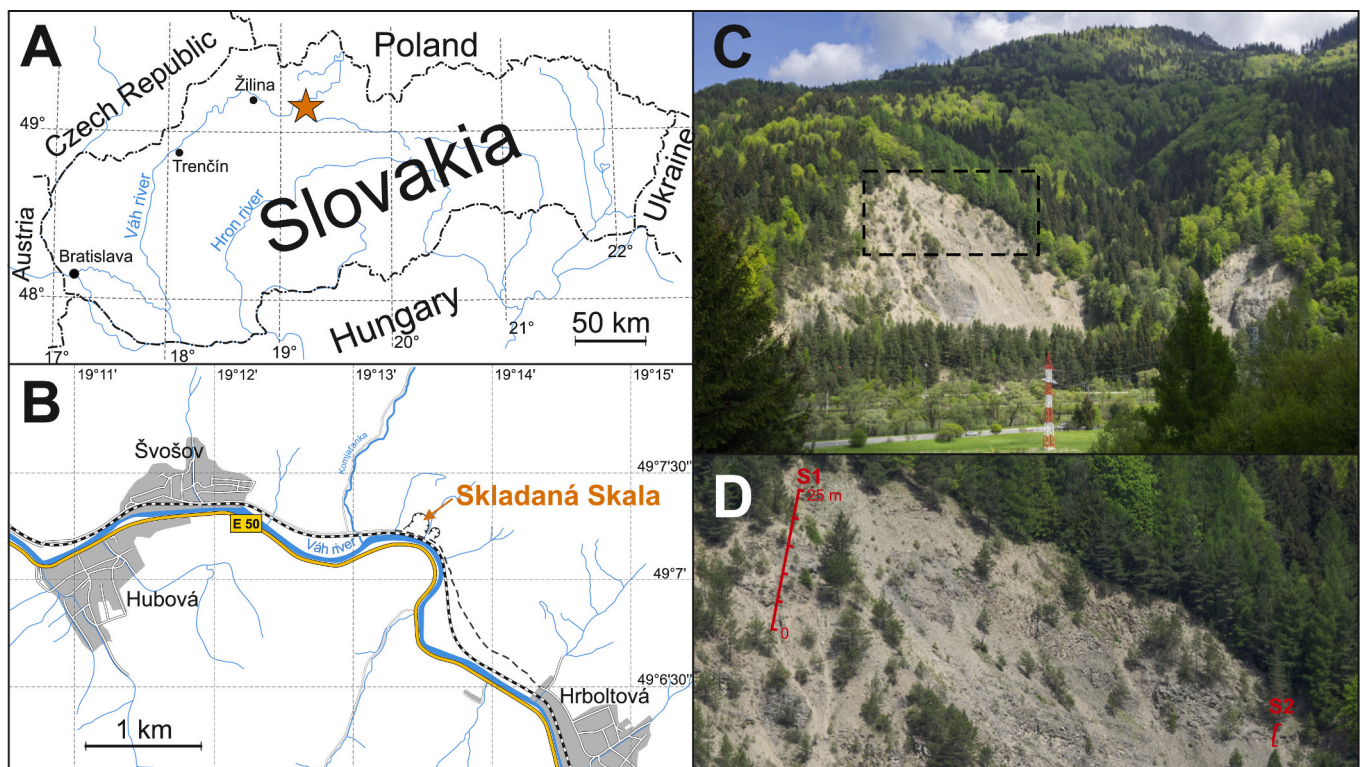


Fig. 2. A: Location of the Skladaná Skala section in Slovakia (orange star). B: Magnified map of the section's locality and surroundings. C: The abandoned Skladaná Skala quarry (Velká Fatra Mountains) where the upper Pliensbachian-lower Toarcian successions with the T-OAE are exposed. D: Closer view of the locations of S1 and S2 sections.

3.1. Geochemical analyses

The carbon and oxygen stable isotope ratios of carbonates were measured using a Gasbench III preparation device coupled to isotope-ratio spectrometer (IRMS) MAT 253 (both Thermo Fisher Scientific). Powdered samples of bulk sediments were loaded into 5 ml borosilicate glass vials (Labco), sealed by caps with rubber septa and flushed with helium to remove atmospheric gases. Subsequent acid digestion (McCrea, 1950) took place at 40 °C overnight. The evolved CO₂ gas was analyzed in continuous-flow mode in helium as carrier gas. In each run, three reference gas peaks were followed by four pulses of sample CO₂. Raw isotope ratios were calibrated using international reference material NBS18 with $\delta^{13}\text{C} = -5.014\text{‰}$, $\delta^{18}\text{O} = -23.2\text{‰}$ and two working standards with $\delta^{13}\text{C} = +2.48\text{‰}$, $\delta^{18}\text{O} = -2.40\text{‰}$ and $\delta^{13}\text{C} = -9.30\text{‰}$, $\delta^{18}\text{O} = -15.30\text{‰}$, respectively. Typical precision of measurement is 0.1‰ for carbon and 0.2‰ for oxygen. Isotope values are reported as permil vs. V-PDB, all the isotope values are reported as permil vs. V-PDB.

Stable carbon isotopes of organic matter were measured on the IRMS MAT253, coupled to elemental analyzer Flash2000 HT Plus (Thermo). Organic residues after digestion in hydrochloric acid of about 60–100 micrograms were wrapped into tin cups and combusted at 1000 °C in quartz tube packed with chromium oxide, electrolytic copper and silvered cobaltous/cobaltic oxide. Purified CO₂ gas was further separated from other gases on capillary GC column (Poraplot Q, Agilent) and lead into IRMS (MAT253) in continuous flow mode in a stream of helium. Raw isotope ratios measured against CO₂ reference gas were calibrated to V-PDB scale using two international reference materials (USGS24 carbon, USGS41 glutamic acid) and two working standards (IVA urea, SUERC carbon) with $\delta^{13}\text{C}$ values -16.05 , $+37.76$, -39.79 , -25.60 , respectively. All the values are reported in permil V-PDB, typical external precision measured on standards is 0.1‰. Bulk rock samples show nine strong outliers in $\delta^{18}\text{O}_{\text{carb}}$ and one outlier in $\delta^{13}\text{C}_{\text{carb}}$ that are strongly negative and exceed the average by more than two standard deviations (Fig. S2). These nine samples tend to have low concentrations of CaCO₃ (four samples in the black shale Bed 64 have depleted values from -9.7 to -11.4‰ , coinciding with $0-7.2\%$ CaCO₃ content) were excluded from analyses. Excluding these samples, $\delta^{18}\text{O}_{\text{carb}}$ and $\delta^{13}\text{C}_{\text{carb}}$ values do not show any positive correlation as would be predicted under meteoric diagenesis (Marshall, 1992); in fact, the correlation is significantly negative (Pearson $r = -0.52$, $p < 0.001$).

The TIC/TOC (total inorganic carbon/total organic carbon) ratios were measured on elemental analyzer Ströhlein C-MAT 5500. Pulverized samples were split into two aliquots of which one was digested in HCl, ca. 50 mg of both were combusted in temperature range 50–1000 °C, evolved CO₂ was measured by infrared detector and carbon content calculated. The TIC/TOC concentrations were calibrated using pure CaCO₃ and accuracy was verified using set of international standards GM, BM, K1, K2, K3 with TIC/TOC 0.07/0.08, 0.40/0.10, 1.88/0.47, 11.92/0.78, and 1.60/3.70, respectively. Precision of measurement in the weight range of our samples is 0.08 wt%.

3.2. Nannofossil preparation

Smear slides for the analysis of calcareous nannofossils from the interval comprised between the base of the section up to 14.43 m were prepared according to the technique described by Bown (1998) at the Université de Lyon. Samples from the upper part of the section were investigated at the Eötvös Loránd University (Budapest) following the same procedure. Smear-slides were prepared from the powdered rock following the technique described by Beaufort (1991) and modified by Geisen et al. (1999). Two grams of material were mixed with a small amount of water and ultrasonicated. The suspended sample was diluted with further 20 ml water and transferred onto the cover slide in a settling device. The water was removed after 2 h of settling time and the air-dried cover slides were mounted on slides as in the standard technique (Bown, 1998). Slides were studied under a polarized optical microscope

at a 1000× magnification. Three traverses of each slide were scanned under a LEICA DM750P microscope (32 mm with a diameter of optical field of view of 200 μm) and all the nannofossils encountered were counted. The smear-slides prepared from the upper part of the section were analyzed under an Olympus BX51 microscope. Assemblage composition and abundance of nannofossils were studied in sixty fields of view per sample.

4. Results

4.1. Lithostratigraphic succession, microfacies and ichnofacies

A ~ 25 m thick composite succession (Figs. 3, S1) (the section S1 is 23.8 m-thick and the section S2 is 3.4 m-thick) exposes the upper Pliensbachian-Toarcian transition and the lowermost Toarcian. It belongs to the Allgäu Formation and is subdivided into four Units: (1) Unit 1 is formed by ~7 m-thick (beds -3 to 44 at S1) alternation of 10–40 cm thick, grey marly limestone and limestone beds, with sporadic ~1–10 cm-thick marly intercalations. Limestones and marly limestones are formed by poorly sorted spiculitic wackestones (Fig. 5), with well-preserved or degraded tubes of the agglutinated foraminifer *Bathysiphon* formed by sponge spicules. Marls are characterized by calcisiltic packstones with worn crinoids. This unit is characterized by a moderately-diverse ichnofauna, with abundant *Zoophycos* (with the burrow diameter up to 5 mm), *Chondrites*, *Lamellaeichnus*, *Teichichnus*, *Palaeophycus*, *Teichichnus*, *Planolites* and *Bathysiphon* (Fig. 5).

(2) In the 4.7 m-thick Unit 2 (Beds 44–63), the thickness of marly limestone beds is reduced to ~10–20 cm and the thickness of marly intercalations increases upwards, up to an 80 cm-thick marl in Bed 61. Limestones still comprise spiculitic wackestones and packstones in the lower part (Fig. 5), whereas radiolarian-spiculitic wackestones and packstones in marly limestone beds 52–62 (similarly as in Unit 1, marly intercalations are formed by microbioclastic crinoidal packstones). Both marly limestones and marls are dominated by *Zoophycos* and *Chondrites*; *Lamellaeichnus*, *Teichichnus*, and *Bathysiphon* are also frequent (Fig. 5). (3) A ~ 60 cm thick, black and finely laminated organic-rich shale (Bed 64) rich in pyrite in the upper 30 cm is well exposed at S2. This layer does not contain any visible trace fossils. (4) Above the black shale, a ~ 8.7 m-thick interval is generally composed of grey-brownish, monotonous fissile marls or marly limestones. Several 5–10 cm-thick marly limestone beds with abundant ammonites occur in the lowermost part of this Unit. The fissile marls and marly limestones are characterized by a poorly-diverse ichnofacies formed by *Chondrites* and by simple, concordantly oriented, 1–2 mm-thick planar and several cm-long burrows of *Zoophycos* (Fig. 5). *Planolites* and *Paleophycus* are less frequent. High abundance of thin burrows and their concordant orientation generate a characteristic, relatively regular fabric formed by mm-scale alternation of light-grey sediment bands and dark-grey burrows. The microfacies are represented by mudstones and wackestones with dispersed worn crinoidal fragments, benthic foraminifers, ostracods, and molluscan fragments. (5) A ~ 6.5 m-thick interval is characterized by the re-appearance of marly limestone beds (Beds 72–89), by low diversity of trace fossils with four taxa, including *Zoophycos*, *Chondrites*, *Planolites* and *Palaeophycus*, and by re-appearance of persistent radiolarians in thin sections. Sponge spicules also re-appear in Bed 72 although their abundance is mostly low. However, in contrast to the units below the black shale bed (Unit 3), units 1 and 2, *Lamellaeichnus* and *Bathysiphon* are missing and density and diversity of trace fossils remains low (Fig. 5). Limestone beds are composed of radiolarian wackestones and packstones in beds 72–87 (Fig. 5). Isolated specimens of *Bositra buchi* occur in Bed 75 and in overlying beds.

4.2. Ammonites

Numerous *Amaltheus* sp. and rare *Leptaleoceras* sp. pointing to the late Margaritatus Zone (Gibbosus Subzone) occur in outcrops below the

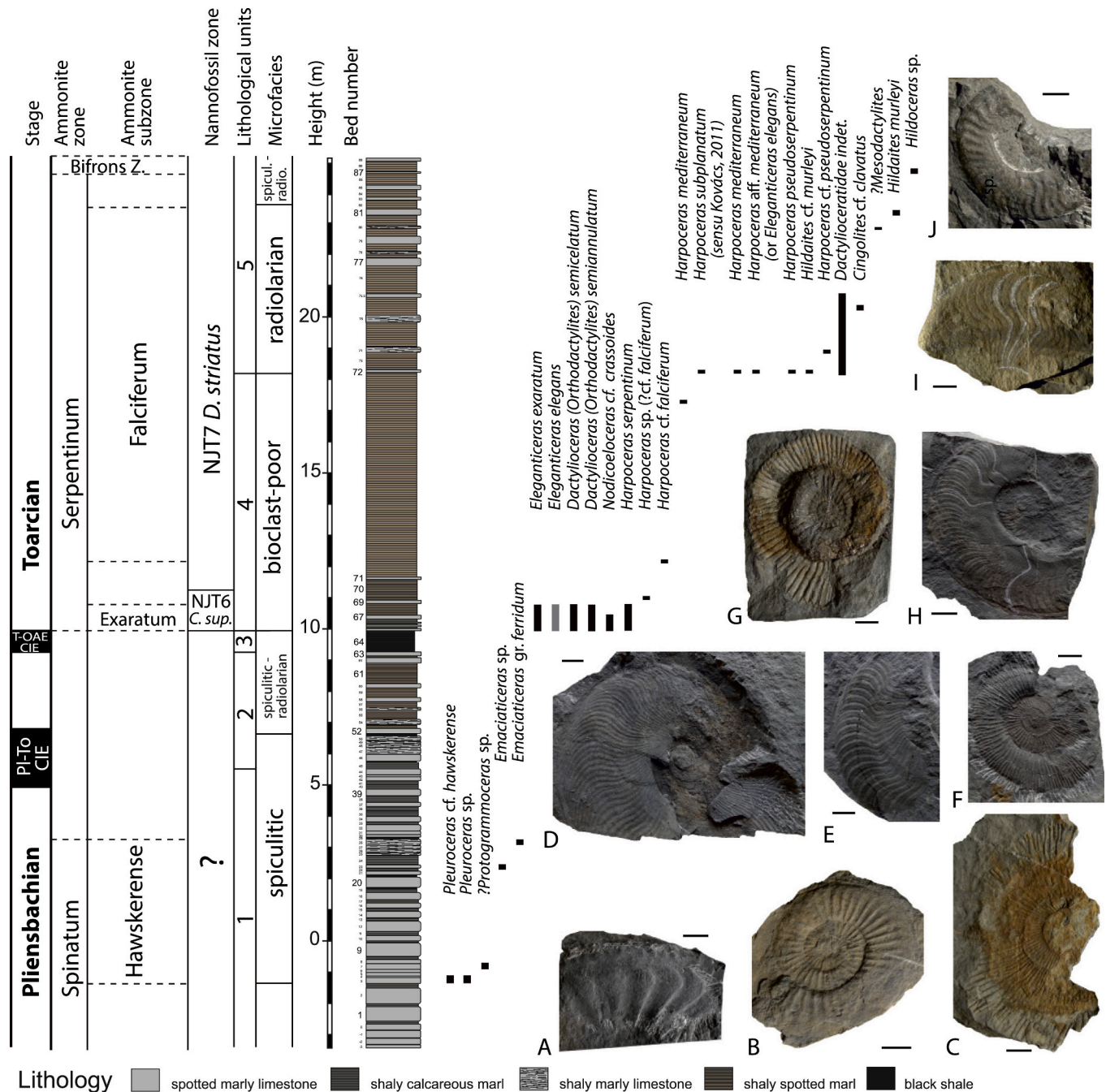


Fig. 3. Composite log, lithology, microfacies, lithological units and biostratigraphic distribution of ammonite taxa in the Skladaná skala section. Ammonites: A. *Pleuroceras* sp., *Emaciaticeras* ex gr. *ferridum*, C. *Dactylioceras (Eodactylites) mirabile*, D. *Eleganticeras elegans*, E. *E. exaratum*, F. *Dactylioceras (Orthodactylites) semiannulatum*, G. *Nodicoeloceras cf. crassoides*, H. *Harpoceras serpentinum*, I. *Harpoceras mediterraneum*, J. *Hildaites cf. murleyi*. Scale bar for ammonites: 10 mm.

measured S1 and S2 sections. Scarce fragments of *Pleuroceras* in Bed 4 and rare *Emaciaticeras* in beds 23 and 28 (section S1) indicate that Unit 1 belongs at least partly to the uppermost Spinatum Zone (Fig. 3). Although the Tenuicostatum Zone of the lower Toarcian is not documented by in situ ammonites, a single specimen of *Dactylioceras (Eodactylites) mirabile* indicative of the lower part of the Tenuicostatum Zone was found in the debris, suggesting that this zone is preserved within Unit 2 between the last occurrence of the late Pliensbachian ammonites in Bed 28 and the earliest ammonites of the Exaratum Subzone at the base of Unit 4 (Fig. 3). The lowermost 1 m of the Unit 4 (section S2) is characterized by abundant ammonites, with *Harpoceras serpentinum*, *Eleganticeras exaratum*, *E. elegans*, *Dactylioceras (Orthodactylites) semicelatum*, and *D. (O.) semiannulatum*. The co-occurrence of

E. exaratum and *E. elegans*, along with *H. serpentinum* in the beds 65–69 indicates that this interval belongs to the middle/upper parts of the Exaratum Subzone (sensu Howarth, 1992a, 1992b) or respectively the upper part of the Elegantulum Subzone (Strangewaysi Horizon, see Elmi et al., 1997). The marly interval just above the Bed 69 (section S2) yielded a fragment of *Harpoceras* sp. with weakly developed lateral spiral groove and falcate ribs. Fragment of *Harpoceras cf. falciferum*, index species of the Falciferum Subzone, was collected in the lower part of the thick marly interval between beds 71 and 72. (section S2). Following taxa were all collected from section S1. The Bed 72 (i.e., the base of Unit 5) is rich in ammonite fragments, mostly of *Harpoceras* ex gr. *mediterraneum* and scarce *Hildaites cf. murleyi*. A single specimen of *Cingolites cf. clavatus* was found in a thin limestone bed situated 50 cm

above Bed 75 and several fragments of *Hildaites* were found in Beds 81 and 83. All these taxa still indicate the Falciferum Subzone of the Serpentinum Zone. Bed 87 contains fragments of *Hildoceras* pointing already to the Bifrons Zone of the middle Toarcian. Occurrence of *Dactyloceras* gr. *commune* was documented ~3.7 m above Bed 85 (after a soil covered interval). The first occurrence of *Dactyloceras* gr. *commune* was found ~3.7 m above Bed 85 (covered interval).

4.3. Calcareous nannofossil

Calcareous nannofossils are extremely rare or not age-diagnostic in the samples studied from the upper Pliensbachian-lowermost Toarcian units 1–2 and in the black shale interval. Nannofossils appear in the interval just above the black shale interval corresponding to the T-OAE and are present, although with low abundances, up to the top of the section (upper part of lower Toarcian and the Bifrons Zone). This increase in abundance of calcareous nannoplankton in wake of the T-OAE is a common trend in many localities from the North margin of the Tethys (Bucefalo-Palliani et al., 2002; Mattioli et al., 2009; Suan et al., 2018).

The earliest event encountered is the first occurrence of the genus

Watznaueria at 10.3 m (right above the black shale unit, Bed 64) with the species *W. fossacincta*, shortly followed by the first occurrence of *W. colacicchii* (Fig. 4). The first occurrence of *Discorhabdus striatus* is recorded 1.3 m above the top of the black shale. This is the marker species of the NJT7 *Discorhabdus striatus* Zone (Bown, 1998; Mattioli and Erba, 1999; Ferreira et al., 2019). Thus, even in the absence of *C. superbus*, which first occurs later in the section, the below interval is assigned to the NJT6 Zone. The base of NJT7 zone corresponds to the upper part of the Falciferum Subzone and coincides with the return to pre-excursion values of the $\delta^{13}C$ after the CIE corresponding to the T-OAE (Ferreira et al., 2019).

4.4. CaCO₃ content and TOC

With the exception of the black shale in Unit 3, the small-scale stratigraphic variability in CaCO₃ content is driven by decimeter-scale alternation of limestones and marls, with median values in limestones attaining 58–73% and in marls attaining 34–45%. At the scale of the five stratigraphic units, median TOC gradually increases from 0.22% in Unit 1 (Spinatum Zone) to 0.32% in Unit 2, markedly increases in the black shale to 1.6% (with 3.3% at maximum), and drops to 0.37% and 0.31%

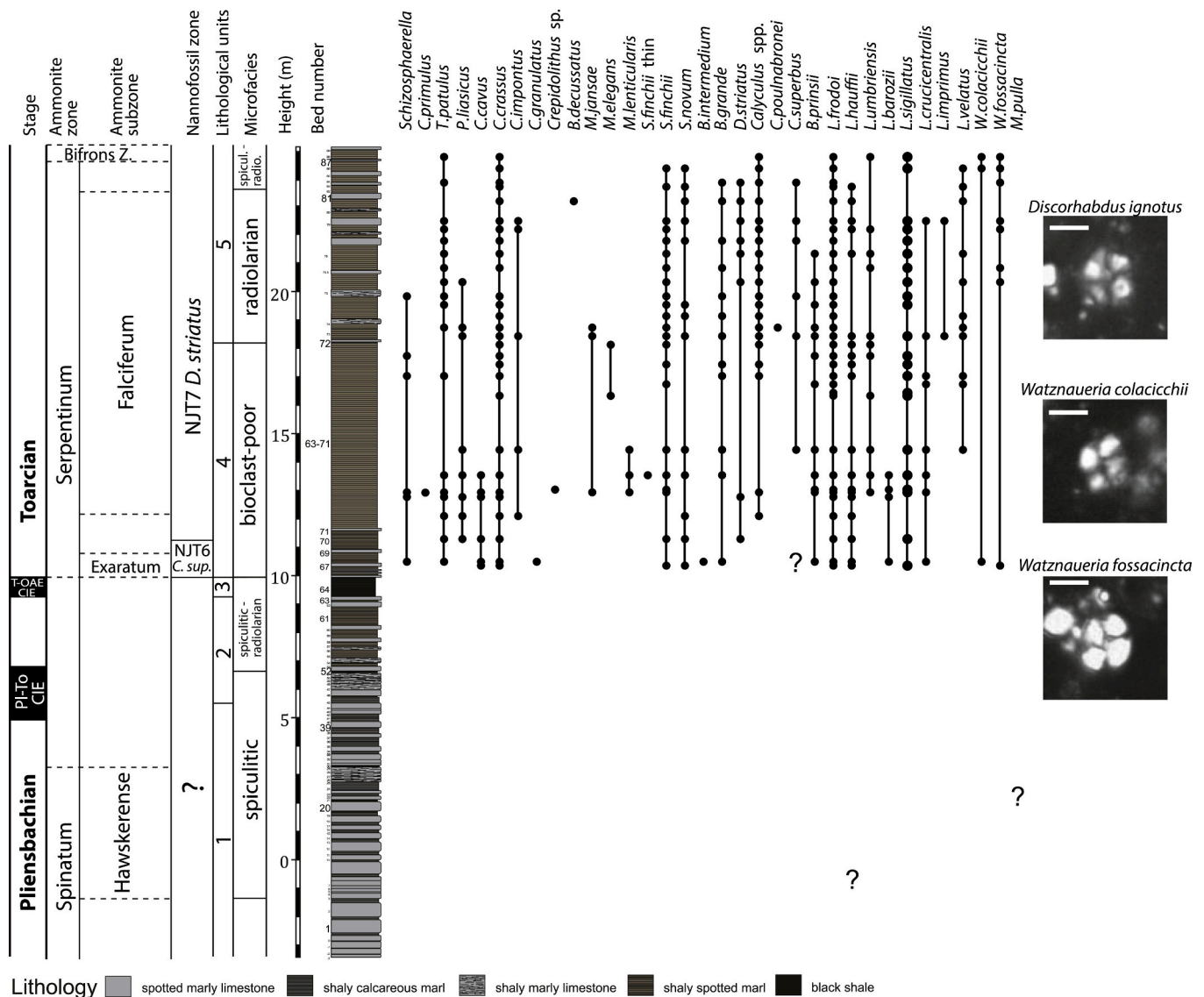


Fig. 4. Composite log, lithology, microfacies, lithological units and biostratigraphic distribution of nannofossil taxa in the Skladaná skala section. Scale bar for nannofossils: 5 μ m.

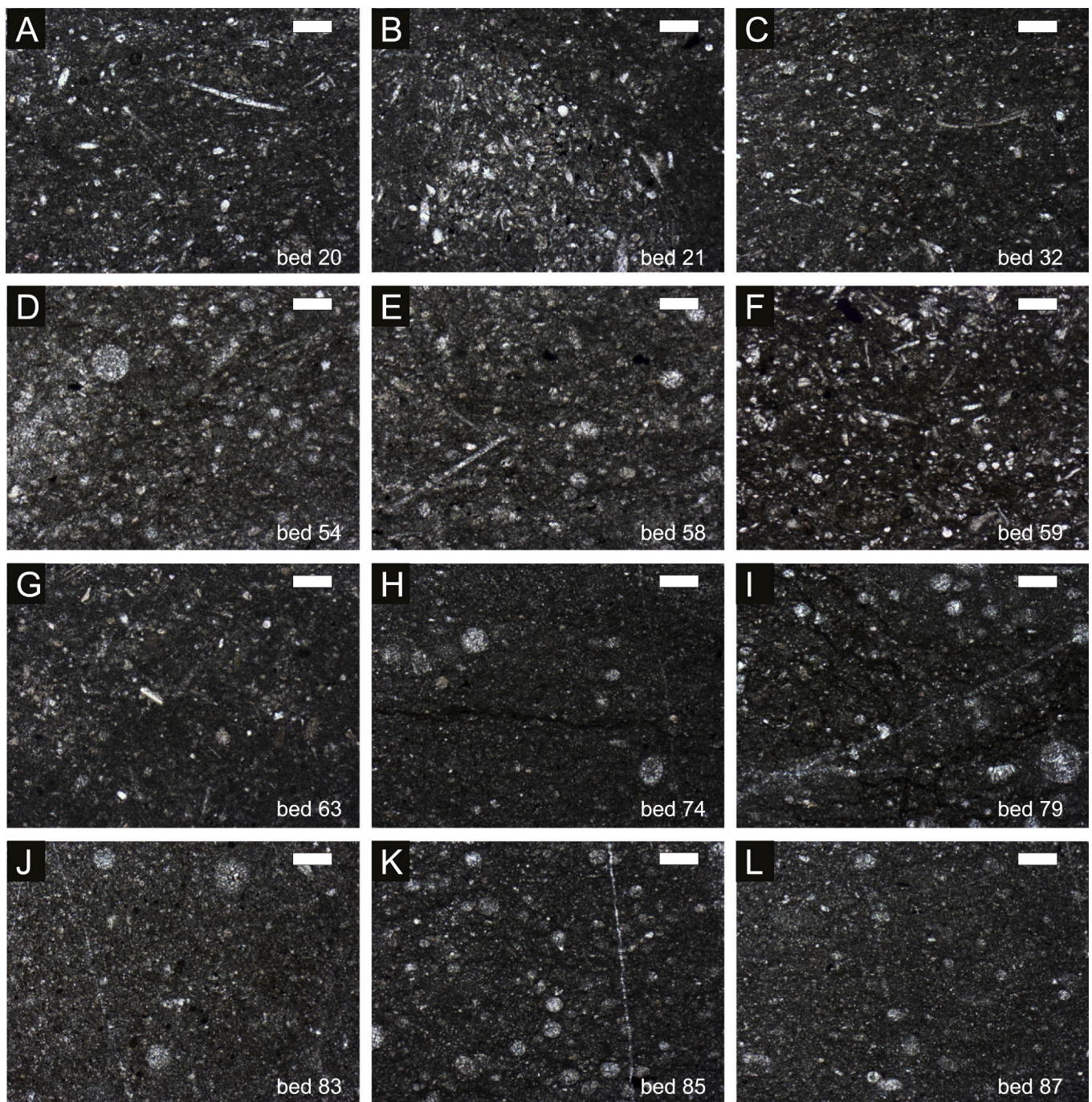


Fig. 5. Stratigraphic changes in microfacies composition, with spiculitic wackestones and packstones with *Bathysiphon* in the Spinatum Zone (A-C, Unit 1) shifting to of spiculitic-radiolarian microfacies in beds 52–63 (D-G, Unit 2). Bioclast-poor mudstones and wackestones occur in Unit 4 (beds 65–71) immediately above the black shale (T-OAE). Radiolarian mudstones and wackestones in the upper part of the Serpentinum Zone in Unit 5 (H-L). Scale bars: 0.2 mm.

in Units 4 (Exaratum Subzone) and 5 (Falciferum Subzone and Bifrons Zone), respectively (Fig. 7 and Table S1). Median CaCO_3 gradually declines from 56% in Unit 1 to 49% in Unit 2, markedly declines to 7% in the laminated black shale (Unit 3), and rebounds to 46% and 38% in Units 4 and 5, respectively. With the exception of the black shale in Unit 3, the overall stratigraphic decline in CaCO_3 and the increase in TOC are primarily driven by an increasing proportion of clay and declining proportion of limestones, rather than by changes in concentrations of CaCO_3 and TOC within marls or within limestone beds. However, CaCO_3 still declines significantly within the marls upsection, from ~45% in Unit 1 to ~35% in Unit 5 (Mann-Kendall trend test, $p = 0.002$). In contrast, CaCO_3 concentrations within the limestones do not change

upsection (Mann-Kendall trend test, $p = 0.11$).

4.5. Carbon and oxygen isotopes

The bivariate relationship between $\delta^{18}\text{O}_{\text{carb}}$, $\delta^{13}\text{C}_{\text{carb}}$ and $\delta^{13}\text{C}_{\text{org}}$ shows that samples fall into two main groups according to their stratigraphic position. The samples from the pre-T-OAE units 1–2 are characterized by more positive $\delta^{18}\text{O}_{\text{carb}}$ and more negative $\delta^{13}\text{C}_{\text{carb}}$ and $\delta^{13}\text{C}_{\text{org}}$, whereas the samples from the post-T-OAE units are characterized by more negative $\delta^{18}\text{O}_{\text{carb}}$ and more positive $\delta^{13}\text{C}_{\text{carb}}$ and $\delta^{13}\text{C}_{\text{org}}$ (Fig. 8 and Table S1). With the exception of the black shale where the carbonate phase is subordinate and does not allow reliable

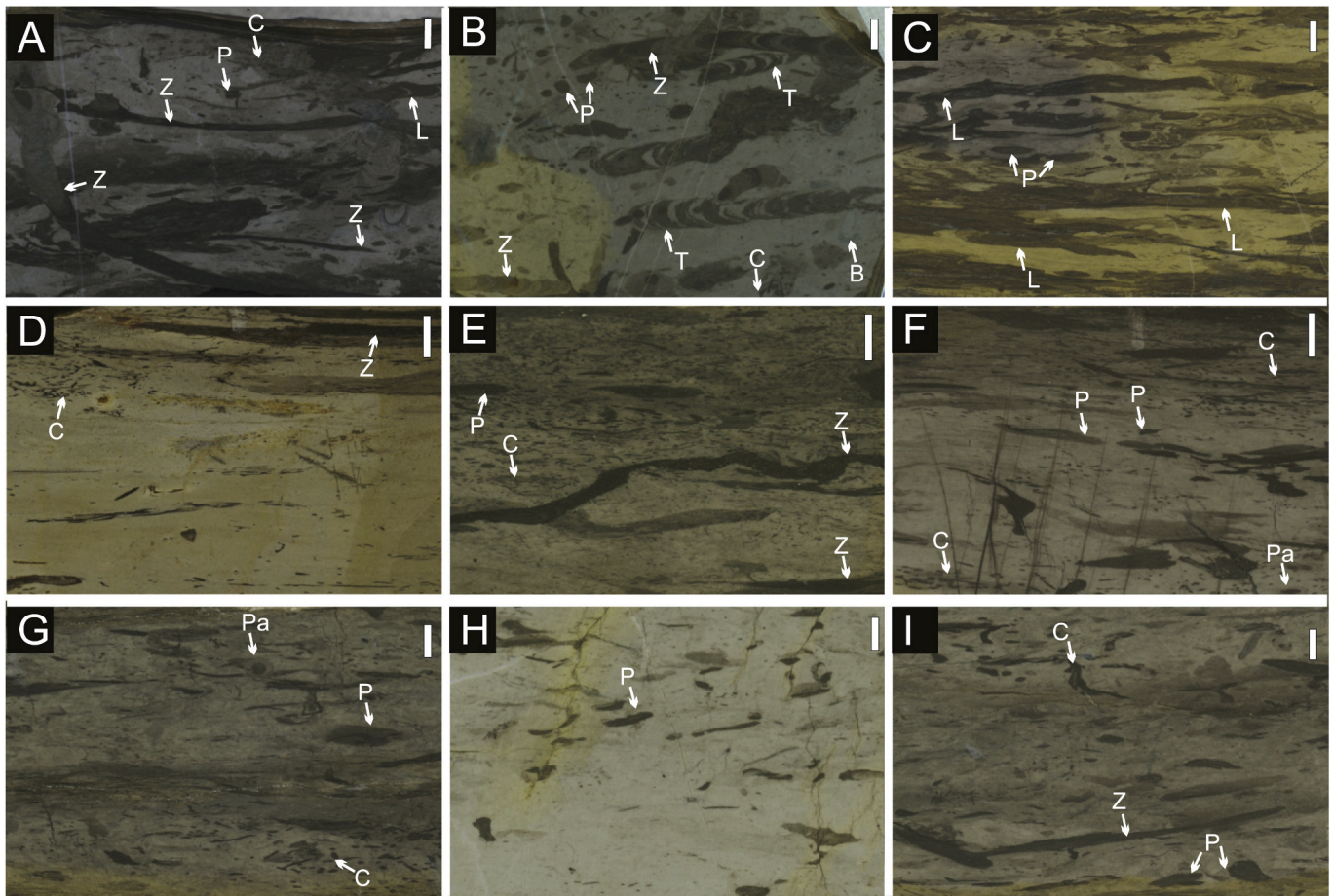


Fig. 6. Trace-fossil assemblages in polished cross-sections showing the transition from pre-extinction ichnofacies with diverse trace fossils in units 1 and 2 (A–C) to the post-extinction ichnofacies in Unit 4 (D–F) and in Unit 5 (G–I). A. Limestone bed 21 with *Lamellaeichnus*, *Zoophycos*, *Chondrites* and *Planolites*. B. Limestone bed 37 with abundant *Teichichnus*. C. Fissile marly limestone bed 49 with abundant *Lamellaeichnus*. D. Marly bed with *Chondrites* and thin burrows of *Zoophycos*, 167 cm above the top of bed 67. E. Marly bed with abundant *Chondrites*, 165 cm above the top of bed 67. F. Marly limestone bed 69 with abundant *Planolites*. G. Limestone bed 74 with abundant *Chondrites* and *Planolites*. H. Limestone bed 79 with abundant *Planolites*. I. Limestone bed 85 with abundant *Zoophycos*, *Planolites*, and *Chondrites*. Labels: Z–*Zoophycos*, C–*Chondrites*, P–*Planolites*, Pa–*Palaeophycus*, L–*Lamellaeichnus*, T–*Teichichnus*. Vertical scale bar: 5 mm.

measurements, $\delta^{13}\text{C}_{\text{carb}}$ and $\delta^{13}\text{C}_{\text{org}}$ show similar trends that can be subdivided into four phases: Phase 1. Stable values in $\delta^{13}\text{C}_{\text{carb}}$ and $\delta^{13}\text{C}_{\text{org}}$ in Unit 1, with $\delta^{13}\text{C}_{\text{org}}$ fluctuating around -27.6‰ and $\delta^{13}\text{C}_{\text{carb}}$ around $1\text{--}1.5\text{‰}$, without any clear trend. The decimeter-scale variability in $\delta^{13}\text{C}_{\text{org}}$ shows high-frequency fluctuations by $\sim 2\text{‰}$. This variability is associated with a gradual decline in $\delta^{18}\text{O}_{\text{carb}}$, declining on average from $\sim -3.1\text{‰}$ to $\sim -4\text{‰}$, with a relatively large scatter between -2.3‰ – -4.9‰ (Fig. 7 and Table S1). Phase 2. A clear negative excursion in $\delta^{13}\text{C}_{\text{carb}}$ by $\sim 0.8\text{‰}$ (minimum = 0.4‰) and a minor excursion in $\delta^{13}\text{C}_{\text{org}}$ can be observed between 4.9 and 7.1 m in beds 40–54, at the boundary between Units 1 and 2. The location of this excursion between the last occurrences of ammonites from the Spinatum Zone and the first appearance of ammonites of the Exaratum Subzone (about 4 m below the main negative CIE, phase 4 below) indicates that it corresponds to the Pliensbachian/Toarcian transition interval (Fig. 7). The $\delta^{13}\text{C}_{\text{org}}$ record shows a mild excursion by 0.5‰ that is not as strong as reported at other sites (Littler et al., 2010; Bodin et al., 2016). The $\delta^{18}\text{O}_{\text{carb}}$ further declines by $\sim 1\text{‰}$ at $\sim 5.9\text{--}8\text{ m}$ above the Pliensbachian/Toarcian transition interval (Beds 54–59). Phase 3. This is the first phase of the positive CIE in Unit 2, with $\delta^{13}\text{C}_{\text{carb}}$ increasing from 0.5‰ to 1.5‰ and $\delta^{13}\text{C}_{\text{org}}$ increasing from -28‰ to -26‰ up to Bed 61. Phase 4. A sharp negative CIE in organic matter of $\sim 5\text{‰}$ between ~ 9.2 and $\sim 11.3\text{ m}$ is detected in the black shale (Unit 3), reaching a minimum of -30.9‰ at $\sim 9.8\text{ m}$ in the upper, pyrite-rich part of Bed 64 (Fig. 7). $\delta^{18}\text{O}_{\text{carb}}$ values sharply decline by 1.5‰ between the pre-T-OAE beds and post-T-OAE

beds within the Exaratum Subzone (Beds 65–68), with the minimum of -5.7‰ .

Phase 5. This second phase of the positive CIE, dated to the NJT7 nanofossil zone, shows a gradual increase from 1.5‰ up to 2.5‰ in $\delta^{13}\text{C}_{\text{carb}}$, and from -27‰ up to 25‰ in $\delta^{13}\text{C}_{\text{org}}$, with the highest values in the upper parts of Unit 4 at $\sim 15\text{ m}$, followed by a gradual reversal towards more negative values in Unit 5. A short negative excursion in $\delta^{13}\text{C}_{\text{carb}}$ by $\sim 1.8\text{‰}$ interrupts the general declining trend in the upper Falciferum Subzone at $20.5\text{--}22.3\text{ m}$ (Fig. 7). The $\delta^{18}\text{O}_{\text{carb}}$ record displays a mild positive trend upsection with gradually decreasing values by $\sim 1\text{‰}$ to the top. This trend is interrupted by a $\sim 1.5\text{‰}$ negative excursion between 20.5 and 22.3 m , at the same level where the $\delta^{13}\text{C}_{\text{carb}}$ shows a negative anomaly (Fig. 7).

5. Discussion

5.1. Preservation of the isotopic signal

The isotopic signals obtained from the samples of the Skladaná Skala section are well-preserved with the exception of samples from the black shale (Bed 64). Nevertheless, thin calcite veins might appear in some beds, they were carefully avoided during the sample preparation, furthermore thin-section observations do not indicate any alteration of the micrite to microsparite (with the exception of μm -scale overgrowths on nanofossils) or to coarser late-diagenetic cements. Although

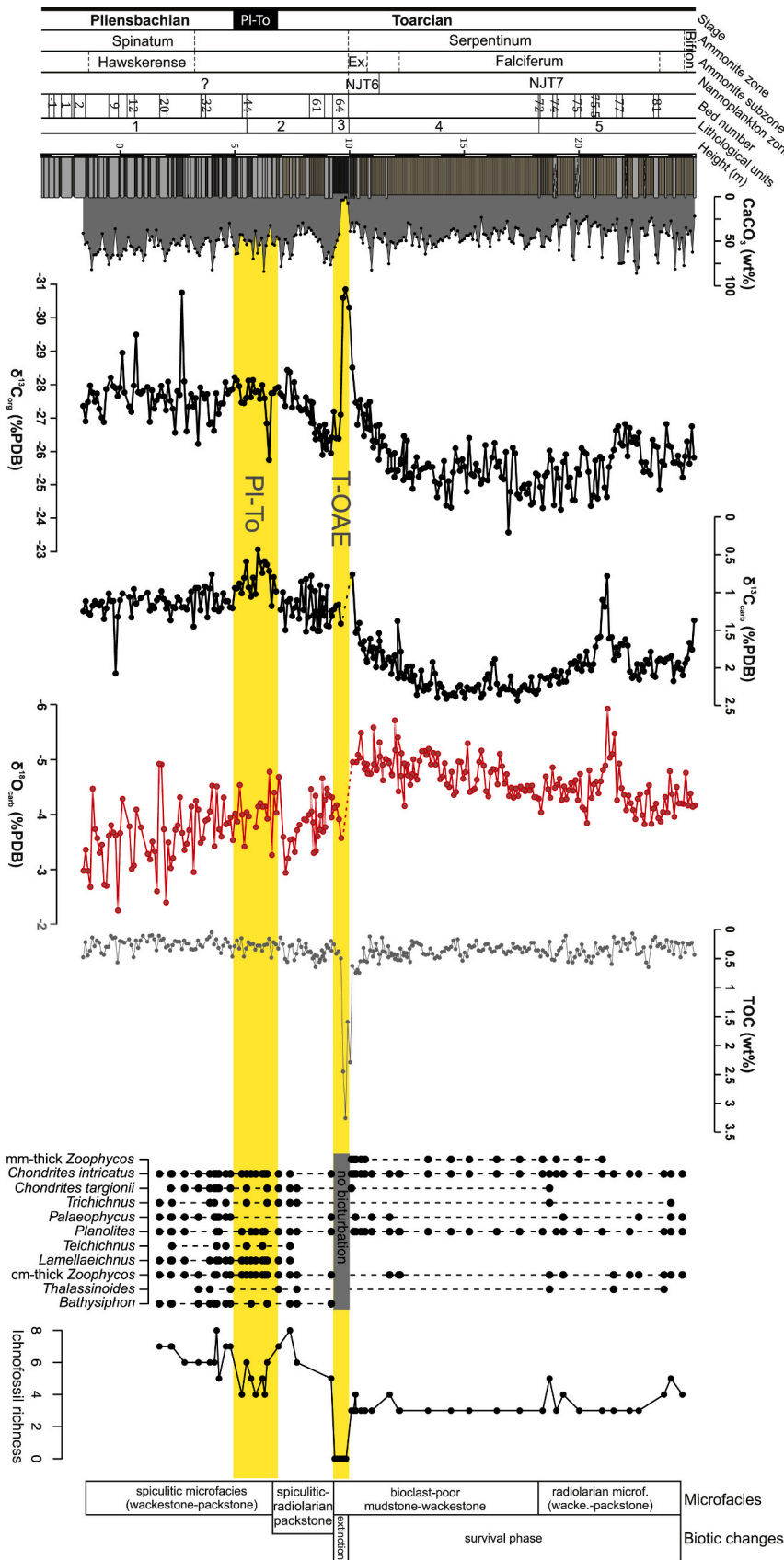


Fig. 7. High resolution CaCO_3 , $\delta^{13}\text{C}_{\text{org}}$, $\delta^{13}\text{C}_{\text{carb}}$, $\delta^{18}\text{O}_{\text{carb}}$ and TOC data from the upper Pliensbachian–lower Toarcian succession at Skladaná Skala. Data points of $\delta^{13}\text{C}_{\text{carb}}$ and $\delta^{18}\text{O}_{\text{carb}}$ from the T-OAE level were excluded from the record because primary carbonate is negligible and the negative $\delta^{13}\text{C}_{\text{carb}}$ and $\delta^{18}\text{O}_{\text{carb}}$ values reflect microscopic calcite veins. Right side: distribution of trace fossils and microfacies changes indicate that the recovery in taxonomic richness of trace fossils was delayed during the Serpentinum Zone. The loss of bioturbation in Bed 64 coinciding with the negative CIE and very small concentrations of CaCO_3 marks the extinction phase, followed by very limited bioturbation in the Exaratum and Falciferum subzones.

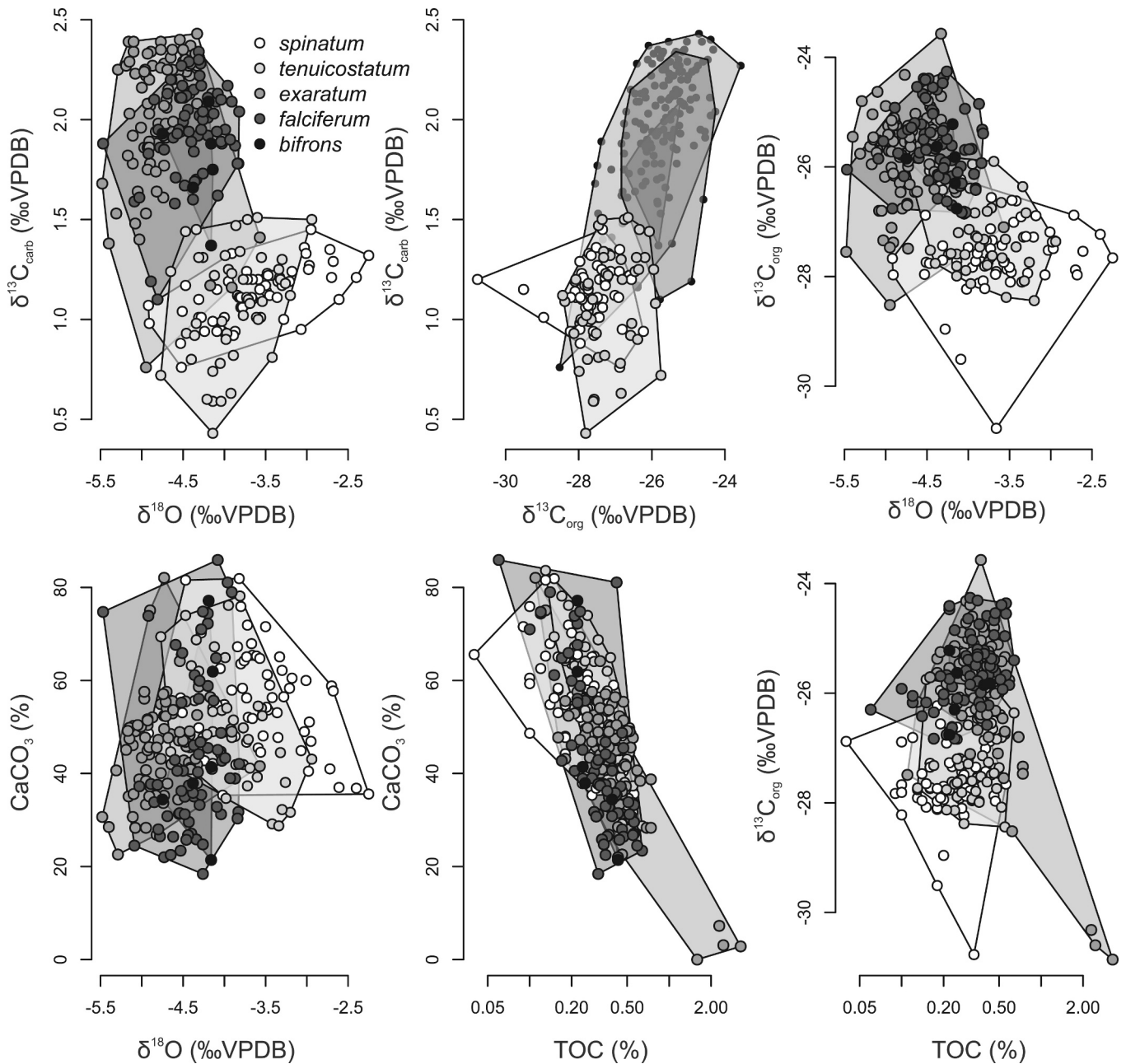


Fig. 8. Major stratigraphic difference in stable isotopic composition of carbonates and organic matter at the boundary between the Tenuicostatum Zone and the Exaratum Subzone (corresponding to the boundary between the units 2 and 3) applies not only to $\delta^{13}\text{C}_{\text{carb}}$ and $\delta^{13}\text{C}_{\text{org}}$ but also to $\delta^{18}\text{O}_{\text{carb}}$. In contrast, the difference does not propagate to differences in TOC (with the exception of the black shale unit). Carbon isotopes and CaCO_3 in the upper parts show a reversal to some degree but do not fully recover to pre-T-OAE values.

$\delta^{18}\text{O}_{\text{carb}}$ from the black shale level are very negative (below -9‰), this level contains very little amount of carbonate (0–7 wt%) and contains only very thin (< 1 mm) calcite veins that likely determined the highly negative $\delta^{18}\text{O}_{\text{carb}}$. Therefore, $\delta^{13}\text{C}_{\text{carb}}$ and $\delta^{18}\text{O}_{\text{carb}}$ data from this level were excluded from interpretation. Meteoric diagenesis tends to shift $\delta^{13}\text{C}_{\text{carb}}$ and $\delta^{18}\text{O}_{\text{carb}}$ to negative values (Marshall, 1992), but the bivariate relation between $\delta^{13}\text{C}_{\text{carb}}$ and $\delta^{18}\text{O}_{\text{carb}}$ does not show any positive correlation (excluding ten outliers specified in Methods, Pearson $r = -0.52$, $p < 0.001$, Fig. S2). The only exception is the anomaly in the Unit 5 with highly negative $\delta^{18}\text{O}_{\text{carb}}$, probably reflecting local diagenetic overprint. The general stratigraphic correspondence between negative and positive phases in $\delta^{13}\text{C}_{\text{carb}}$ and $\delta^{13}\text{C}_{\text{org}}$ indicates that stratigraphic trends in $\delta^{13}\text{C}$ of both components are not biased by diagenetic effects. The five isotopic phases based on positive and

negative $\delta^{13}\text{C}$ anomalies do not have any counterparts in the record of $\delta^{18}\text{O}_{\text{carb}}$, and absolute values in $\delta^{18}\text{O}_{\text{carb}}$ are likely biased by lithification towards more negative values as is typical of bulk-sample measurements, but the abrupt and persistent shift towards negative values between units 1–2 on one hand and units 4–5 on the other hand is not associated with any major facies or diagenetic change, and can reflect a shift towards warmer bottom-water temperatures during the T-OAE as observed in other well-preserved sections.

5.2. Pliensbachian/Toarcian boundary negative CIE and the first phase of positive CIE

A distinct negative excursion in $\delta^{13}\text{C}_{\text{carb}}$ by $\sim 0.8\text{‰}$ between 4.9 and 7.1 m (Fig. 7) is located ~ 2 –4 m above the last occurrence of ammonites

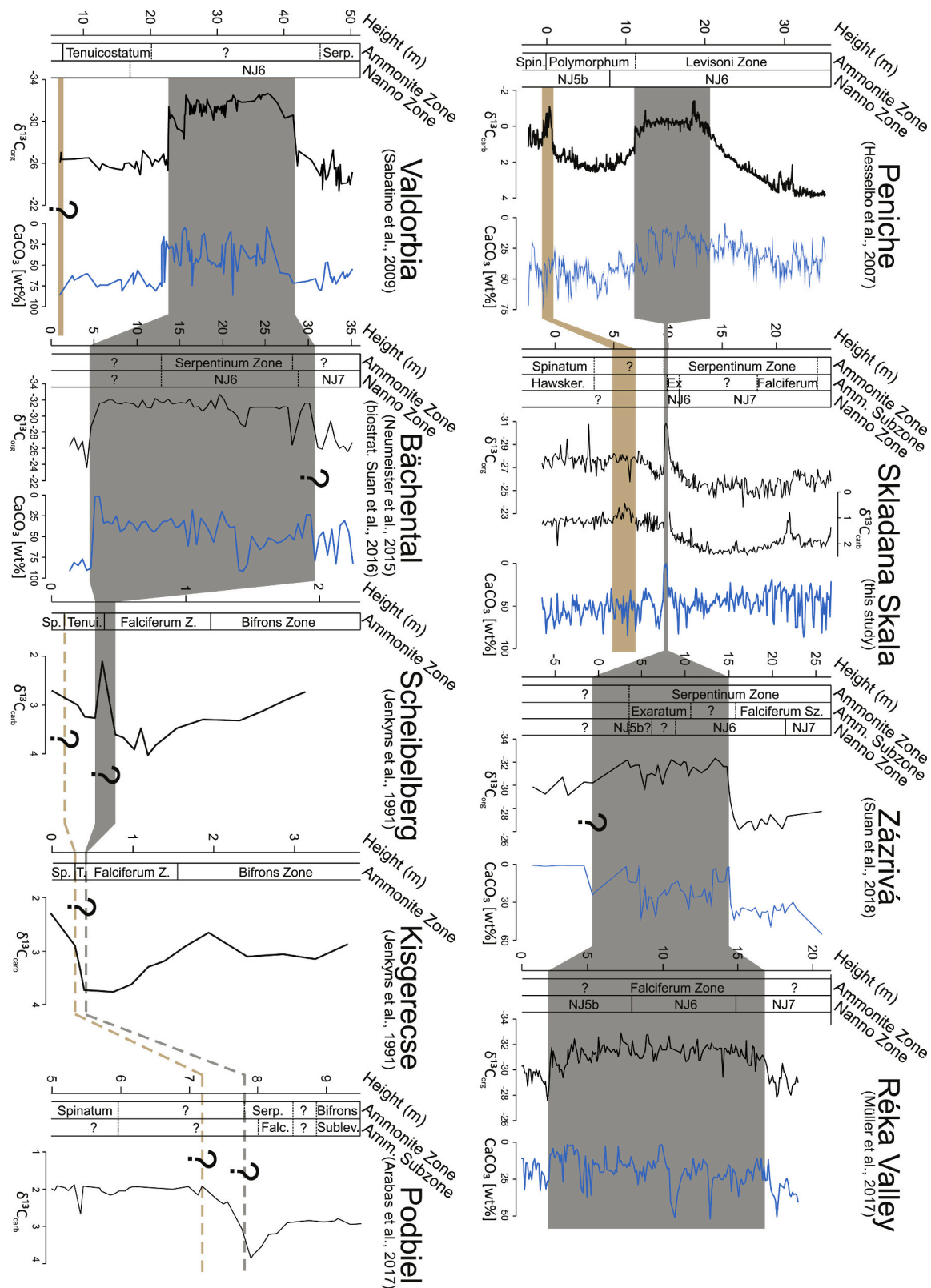


Fig. 9. Carbon isotope chemostratigraphic correlation of Skladaná Skála with the Peniche GSSP section from the Lusitanian basin (Hesselbo et al., 2007) and with few of the key NW Tethyan sections used in this study: Zázrivá from Pieniny Klippen Belt (Suan et al., 2018); Réka Valley from Mecsek Zone of the Tisza Unit (Müller et al., 2017); Valdorbria from Umbria-Marche (Sabatino et al., 2009), Bächental and Scheibelberg, Northern Calcareous Alps (Neumeister et al., 2015; Suan et al., 2016; Jenkyns et al., 1991), Kisgerecse, Transdanubian Unit (Jenkyns et al., 1991); Podbien, Pieniny Klippen Belt (Arabas et al., 2017). Grey band is marking the correlation of the T-OAE and brown one the PI-To negative CIE. Question marks are indicating uncertain levels in correlation. CaCO₃ data from sections where it was available is presented (blue lines). (For interpretation of the references to colour in this figure legend, the reader is referred to the web version of this article.)

of the Spinatum Zone in bed 28. The chemostratigraphic record of the Pl-To negative carbon excursion observed in other regions indicates that the anomaly starts already in the uppermost Pliensbachian (Fig. 7, see also Littler et al., 2010; Trecalli et al., 2012; Bodin et al., 2010, 2016; Ait-Itto et al., 2017; Menini et al., 2019; Ferreira et al., 2019), suggesting that the Pliensbachian/Toarcian boundary transition interval is located at 4.9–7.1 m based on the $\delta^{13}\text{C}_{\text{carb}}$ curve (Fig. 7). This prominent CIE of the Pliensbachian/Toarcian boundary has been reported from different regions from bulk, belemnite and brachiopod carbonate and also from bulk organic matter and fossil wood, usually showing a negative shift in a range of 2–4‰.

The negative CIE at the Pliensbachian/Toarcian boundary probably marks the onset of release of greenhouse gases through volcanism of the Karoo-Ferrar LIP (precursor activities before the main phase coinciding with the T-OAE) or by methane-hydrate release (Jenkyns and Clayton, 1997; Hesselbo et al., 2007; Suan et al., 2010; Littler et al., 2010; Bodin et al., 2016; Ait-Itto et al., 2017; Menini et al., 2019), and is thus dynamically linked with the T-OAE. Although this excursion marks the onset of elevated benthic extinctions at provincial or global scales (Harries and Little, 1999; Caruthers et al., 2013), it did not seem to markedly affect hemipelagic settings in the Tethys Ocean. The diversity of trace fossils and the ichnofabric in Unit 2 remains similar or slightly declines relative to Unit 1, although the assemblage becomes more dominated by *Zoophycos*. This interval also coincides with a relatively abrupt appearance of abundant radiolarians, forming spiculitic-radiolarian packstones in beds 52–62, but this microfacies shift probably reflects the rapid sea-level rise close to the Pliensbachian/Toarcian boundary as also observed in other Tethyan basins (Hardenbol et al., 1998; Pittet et al., 2014), leading to the deepening of the depositional environment. The lack of strong response can be partly explained by dysoxic bottom-water conditions that characterized the deposition of spotted marls and limestones with thin fully-mixed layer above the redoxcline and inefficient mixing organic-rich sediment below it, typical of semi-enclosed hemipelagic basins with limited ventilation (Šimo and Tomašových, 2013; Reolid and Reolid, 2020). Spotted marls and limestones are typically dominated by remains of siliceous sponges and by agglutinated foraminifers (*Bathysiphon*), and carbonate producers such as mollusks, brachiopods or echinoderms are very rare (Šimo and Tomašových, 2013).

The duration of the Pliensbachian/Toarcian negative CIE is estimated to be ~120–240 kyr (Bodin et al., 2016; Ait-Itto et al., 2018; Boulila et al., 2019). Therefore, the small magnitude of the 0.8‰ negative excursion at the Pliensbachian/Toarcian boundary can be subdued owing to regional factors resulting in smaller carbon isotope fractionation or by reduced net sedimentation rate (Bodin et al., 2016; Ait-Itto et al., 2018; Boulila et al., 2019). The $\delta^{13}\text{C}_{\text{org}}$ record at Skladaná Skala shows an even milder excursion relative to the excursion in $\delta^{13}\text{C}_{\text{carb}}$ (Fig. 7), resembling the record without any sharp excursion in $\delta^{13}\text{C}_{\text{org}}$ at the Amellago section in the Central High Atlas in Morocco (Bodin et al., 2016). The subtle nature of the $\delta^{13}\text{C}_{\text{org}}$ excursion can be related to enhanced contribution of terrestrial organic matter (van de Schootbrugge et al., 2013; Suan et al., 2016). However, Unit 2 shows a trends towards positive values, that is reflected by both $\delta^{13}\text{C}_{\text{org}}$ and $\delta^{13}\text{C}_{\text{carb}}$, corresponding to the first phase of the long-term positive CIE.

5.3. Early Toarcian negative CIE excursion

The onset of the negative CIE associated with the T-OAE is defined as the first significant drop in $\delta^{13}\text{C}$ in the upper part of the Tenuicostatum Zone and the rebound is defined as the inflection point to more positive values in the Serpentinum Zone in NW European sections (Fig. 7, Hesselbo et al., 2007; Bodin et al., 2016). The $\delta^{13}\text{C}_{\text{org}}$ values at Skladaná Skala show both an onset and rebound of negative values between 9 and 10.3 m. The prominent negative excursion by ~5‰, and the most negative values (–30 to –31‰) are limited to 40 cm-thick uppermost, laminated and pyrite-rich part of the black shale (Bed 64) (Fig. 7).

Ammonites of the Exaratum subzone occur in beds that immediately overlie the black shale, confirming that the negative excursion in $\delta^{13}\text{C}_{\text{org}}$ corresponds to the T-OAE. The magnitude of the $\delta^{13}\text{C}_{\text{org}}$ negative CIE (~5‰) and the most negative values (–30 to –31‰) (Fig. 7) at Skladaná Skala are equivalent to the magnitude of CIE observed in other Tethyan and NW European epicontinental settings (Sabatino et al., 2009; Neumeister et al., 2015; Suan et al., 2015; Müller et al., 2017; Ruebsam et al., 2018; Xu et al., 2018). Similarly as in other regions, the main negative CIE is associated not only with the absence of burrowing benthic fauna but also with the significant reduction in carbonate input, showing that the defaunation (i.e., extinction phase) and the collapse of carbonate production is also expressed in the stratigraphic record of hemipelagic basins in the Central Western Carpathians.

5.4. Second phase of positive CIE excursion

Both the $\delta^{13}\text{C}_{\text{org}}$ and $\delta^{13}\text{C}_{\text{carb}}$ curves show a broad positive CIE in the lower Toarcian at Skladaná Skala, which is interrupted by the negative CIE of the T-OAE (Fig. 7). The second phase of the positive CIE, starting immediately above the black shale, spans the Exaratum Subzone and the NJT6 in the lowermost part, and the Falciferum and the NJT7 in the middle and upper parts, in line with other records in various Tethyan localities (Ferreira et al., 2019). This character of the lower Toarcian carbon isotope record indicates widespread, enhanced organic matter production and burial resulting in the depletion of ^{12}C in the global carbon pool during the Tenuicostatum and Falciferum zones, terminating close to the beginning of the Bifrons Zone (Jenkyns et al., 1991; Jenkyns et al., 2002; Hermoso et al., 2013). The full preservation of the positive CIE at Skladaná Skala indicates that sedimentation rates were higher relative to the T-OAE interval, and the effects of local factors (that modulated the expression of the negative excursion at the Pliensbachian/Toarcian boundary) did not confound the expression of the global cycle. Trace-fossil assemblages are effectively limited to four ichnotaxa in units 4 and 5 (i.e., they correspond to survival phase as pre-extinction diversity levels are higher), represented primarily by *Chondrites* and by thin *Zoophycos*, and by less frequent *Planolites* and *Paleophycus* (Fig. 6). Bioclast-poor microfacies in Unit 4, with worn crinoidal fragments, foraminifers, ostracods and mollusks and without sponge spicules and radiolarians, indicates that the decline in trace-fossil diversity in the wake of the T-OAE is not simply reflecting an increase in water depth (that would predict a direct replacement of spiculitic-radiolarian microfacies by radiolarian microfacies). Therefore, environmental stress, possibly driven by oxygen depletion and by persistently-higher bottom-water temperature, i.e., the two factors that contributed to the T-OAE extinction (Baeza-Carratalá et al., 2015; Dunhill et al., 2018; Rita et al., 2019; Ros-Franch et al., 2019), probably contributed to the delayed recovery in hemipelagic basins of the Central Western Carpathians.

5.5. Reduced input of siliciclastics during the T-OAE

A comparison of the Skladaná Skala sections with other NW Tethyan (oceanic) and epicontinental basins (e.g., Lusitanian Basin) reveals two specific features (Fig. 9). First, the biostratigraphic data and chemostratigraphic correlation of the negative and positive CIEs with other regions indicate that the stratigraphic extent of the T-OAE (Unit 3) is extremely limited in comparison to thickness preserved on epicontinental shelves. At epicontinental shelves that were paleogeographically close to the Central Western Carpathians (Sections 1–2 in Fig. 1B), anoxic sediments exhibiting the negative CIE are significantly thicker. Black shales dated to the Exaratum Subzone exhibit the negative CIE over >10 m in the Pieniny Klippen Belt at Zazrivá (Suan et al., 2018). The entire record of T-OAE with the negative CIE is formed by a ~13 m-thick, laminated black shale unit in the Réka Valley in the Mecsek (Müller et al., 2017) (Fig. 9). These locations were not yet segregated from the European passive margin by other basins and were located

closer to the source of river-borne siliciclastic input. Second, the observation that most of the negative CIE almost fully corresponds to the laminated black shale and that this CIE does not encompass bioturbated sediments indicates strong condensation rather than representing only short-term anoxia. The appearance of *D. striatus* just 1.3 m above the top of the black shale, marking the NJT7 zone correlative of the upper part of the Falciferum Subzone (Bown, 1998; Mattioli and Erba, 1999; Perilli, 2000; Ferreira et al., 2019), indicates that net sedimentation rate was still very low during the alternation of marls and marly limestones (with ammonites of the Exaratum Subzone) just above the black shale. The thickness of Unit 3 is also limited relative to the first and second phase of the long-term positive CIE, represented by ~4.5 m in the lower part (the duration of Tenuicostatum – or Polymorphum – Zone is difficult to constrain, ~0.3–0.8 Myr long; Suan et al., 2008b; Huang and Hesselbo, 2014; Boulila and Hinnov, 2017) and by ~15 m in the upper part (subtracting the duration of the T-OAE, the late Serpentinum Zone can have the duration of ~1 Myr, Boulila et al., 2014). The duration of the entire negative CIE is estimated as ~300–900 kyr on the basis of astronomical calibrations (Suan et al., 2008b; Boulila et al., 2014; Huang and Hesselbo, 2014), this time interval is just preserved in few decimeters at Skladaná Skala. The large magnitude of the CIE indicates that the anomaly is not averaged out by condensation of pre-CIE and CIE deposits or by condensation of CIE and post-CIE deposits, respectively. The slow sedimentation rate was thus not associated with a significant temporal change in the isotopic composition of organic matter deposited on the seafloor. The condensation of the black shale and of the overlying bioturbated sediments of the Exaratum Subzone and of the lower part of the Falciferum Subzone probably includes diastems or short-term hiatuses but they did not leave any geochemical or mineralogical signal as there is no evidence of firmgrounds or hardgrounds.

The condensation of the T-OAE in sections of red nodular limestones that were deposited on pelagic swells (Scheibelberg and Kisgerese, Jenkyns et al., 1991, and Podbiel, Arabas et al., 2017) is not surprising owing to the effects of currents and bypassing. However, the negative CIE in Tethyan oceanic sections shows signs of condensation also in basinal settings. For example, $\delta^{13}\text{C}_{\text{org}}$ record of the Bächtental section in the Northern Calcareous Alps displays a sudden negative shift in the lower Toarcian, marking the onset of the T-OAE (Neumeister et al., 2015), also indicating some degree of condensation at the onset of the negative CIE. The overall condensation during the T-OAE is thus not only driven by (1) the collapse of the hemipelagic carbonate factory but also by (2) starvation of siliciclastic supply. The latter (2) is probably associated with marine transgression concurrent with global warming at the onset of the negative CIE (Pittet et al., 2014; Ruebsam et al., 2019). Even when the T-OAE was in turn characterized by enhanced continental weathering that led to higher clay accumulation rate on epicontinental shelves (Dera et al., 2009; Hermoso and Pellenard, 2014), this effect was probably insufficient to compensate for retrogradation of siliciclastic sediments in oceanic environments. To summarize, the findings of thin T-OAE laminated deposits in hemipelagic basins do not indicate that deeper oceanic habitats represented refugia that were affected by anoxia only for a brief duration.

5.6. Carbonate production setback in NW Tethyan shelf

Sediments at Skladaná Skala are composed of micritic hemipelagic limestones and marls with variable contribution of clay and microcrystalline diagenetic silica, without any silty or coarser siliciclastic fractions (other than clay) that would imply significant terrestrial influence. The initial decline in CaCO_3 within Unit 2, also associated with the increasing proportion of marls, co-varies with the first phase of the CIE. The significant drop in CaCO_3 to 0–7% coinciding with the negative CIE and an increase in TOC in the black shale demonstrates that the carbonate factory suffered a significant setback during the T-OAE, similarly as in other Tethyan regions. Although the deposition of marls with 30–40% of CaCO_3 returned still during the Exaratum Subzone, in

the aftermath of the T-OAE, the deposition of limestone beds with >60% of CaCO_3 was renewed during the late Serpentinum Zone only. A drop in CaCO_3 associated with the T-OAE negative CIE has been identified at numerous locations in NW European epicontinental basins, in Tethyan basins and in carbonate platforms as well, and probably reflects a major calcification crisis (Suan et al., 2008a; Sabatino et al., 2009; Léonide et al., 2012; Suan et al., 2018; Brame et al., 2019). Multiple mutually not exclusive scenarios can explain this calcification crisis, including changes in carbonate saturation level of seawater due to increased emission of CO_2 , temperature rise, and/or eutrophication due to acceleration of hydrological cycle and changes in surface water salinity (Mattioli et al., 2009; Trecalli et al., 2012; Hermoso et al., 2012; Müller et al., 2020). Our record is showing that the calcification crisis severely affected the carbonate factory that was the major source of hemipelagic micritic sediments in a basinal setting in the Central Western Carpathians. In a broader context, the decline in carbonate sedimentation affected large parts of the NW Tethyan shelf. Chemostratigraphic correlation of key NW Tethyan localities, together with available CaCO_3 records indicates that carbonate production decline is similarly closely associated with the onset of the negative excursion in Valdorbja, Réka Valley, and Bächtental (Fig. 9). The condensed nature of the T-OAE at pelagic swells can be partly accounted for by winnowing and sediment bypassing, but the independent evidence for decline in carbonate export in basinal sections indicates that the lack of carbonate sediments also contributes to condensation at Scheibelberg, Kisgerese, and Podbiel (Fig. 9).

5.7. Delayed recovery

The recovery pattern of benthic communities after the T-OAE differed between epicontinental seas with widespread anoxia and basins less affected or unaffected by anoxic conditions. On one hand, benthic communities in the Lusitanian and Iberian basins or in Algeria recovered relatively quickly, still during the Serpentinum Zone (Gahr, 2005; García-Joral et al., 2011; Reolid et al., 2012a, 2012b). In contrast, the Peritethyan or Panthalassan shelf environments were affected by anoxia for longer periods, and the diversity of benthic communities with brachiopods, mollusks, and trace producers was typically delayed into the middle Toarcian, i.e., it occurred during the Bifrons Zone (García-Joral et al., 2011; Martindale and Aberhan, 2017; Caswell and Frid, 2017; Caswell and Dawn, 2019). The slower recovery in those basins can be explained by longer duration of anoxia coupled with the lack of facilitative effects of opportunistic burrowers that can bioirrigate the sediment and increase nutrient recycling. This delayed recovery contrasts with more rapid recoveries that characterized less enclosed shelf and oceanic basins or shallower habitats less exposed to persistent or repeated anoxia (Woodfine et al., 2008; Caswell and Coe, 2012). The loss of trace fossils in the T-OAE black shale and the poorly-diverse ichnofacies (either limited to monotypic *Chondrites* levels or to levels with very thin *Zoophycos*) in the overlying post-extinction strata indicate that although bottom-water conditions were not anoxic in the wake of the T-OAE in the Central Western Carpathians, some degree of oxygen depletion persisted for a significant duration (i.e., Serpentinum Zone) in hemipelagic basins in the. The duration of this survival phase can be also affected by persistence of higher bottom-water temperatures as $\delta^{18}\text{O}_{\text{carb}}$ in units 4–5 are significantly more negative than $\delta^{18}\text{O}_{\text{carb}}$ in units 1–2.

Although the overall replacement of spiculitic microfacies by spiculitic-radiolarian microfacies between units 1 and 2 and the dominance of radiolarian microfacies in Unit 5 may be explained by an increase in water depth (that occurred both during the Pliensbachian/Toarcian boundary and during early Toarcian) and by reduced flux of particulate organic matter required by filter-feeders such as sponges, this explanation does not explain the unique post-extinction pattern observed just above the black shale. First, the presence of bioclast-poor mudstones and wackestones without radiolarians and sponge spicules in Unit 4 shows that the paleoecological trends in microfacies and

ichnofacies cannot be simply explained by an increase in water depth. Second, this shift is associated with a decline in $\delta^{18}\text{O}$ (especially immediately above the beds recording the T-OAE), hence arguing against a simple trend towards deeper and colder water, and average TOC increases slightly from Unit 1 to Unit 4 (excluding Unit 3 from the comparison) indicating that post-event organic flux was not significantly reduced. The microfacies shift is therefore more likely to be related to bottom-water stress that resulted from changes in ventilation and possibly higher bottom-water temperatures.

6. Conclusions

High-resolution geochemical and biostratigraphic data from the limestone-marl succession at Skladaná Skala (Central Western Carpathians, Križna Unit), which was deposited in a relatively deep hemipelagic basin in the Tethys during the Pliensbachian and Toarcian document the negative carbon isotope excursions at the Pliensbachian-Toarcian boundary and in the lower part of the Serpentinum Zone, and the long-term positive CIE terminating close to the Serpentinum/Bifrons zonal boundary. The succession reveals a significant decline in the deposition of carbonate sediments and siliciclastic starvation during the T-OAE, associated with a prominent negative CIE preserved just in a 40 cm-thick laminated black shale. The T-OAE in the oceanic Tethys was thus associated not only with limited carbonate production but also with reduced siliciclastic supply, probably induced by rapid sea-level rise that temporally coincided with the T-OAE. In contrast to the negative CIE, the first and the second phase of the positive CIE was characterized by higher sedimentation rates. Trace-fossil assemblages remained poorly diverse during most of the Serpentinum Zone, and the benthic recovery in terms of diversity of trace fossils did not achieve pre-extinction levels even at the Serpentinum/Bifrons boundary. These results suggest that a calcification crisis during the T-OAE had long-term effects on the hemipelagic ecosystems in the Central Western Carpathians, as well as on the entire NW Tethyan pelagic-hemipelagic carbonate shelf.

Supplementary data to this article can be found online at <https://doi.org/10.1016/j.gloplacha.2020.103366>.

Declaration of competing interest

The authors declare that they have no known competing financial interests or personal relationships that could have appeared to influence the work reported in this paper.

Acknowledgements

We thank for Hana Demeterová for her help in sample preparation and carbon and oxygen isotope analyzes at the laboratory of the Slovak Academy of Sciences. This project was funded by the European Union's Horizon 2020 research and innovation program under the Marie Skłodowska-Curie grant agreement and project BASE-LiNE Earth [No. 643084], by the Slovak Research and Development Agency (APVV 0555-17) and by the Slovak Scientific Grant Agency (VEGA 0169-19). JP received funding by the National Research, Development and Innovation Office of Hungary (Grants OTKA NN 128702 and K 135309). This is a contribution to IGCP Project 655 and MTA-MTM-ELTE Paleo contribution No. 332. EM acknowledges Mrs. Ghislaine Broillet for smear slide preparation. *Slides are curated at the Collections de Géologie de Lyon with an attributed FSL numbering.* The research was also supported by the European Union and the State of Hungary, co-financed by the European Regional Development Fund in the project of GINOP-2.3.2.-15-2016-00009 'ICER'. We also thank to two anonymous reviewers for their constructive comments and suggestions.

References

- Ait-Itto, F.Z., Price, G.D., Addi, A.A., Chafiki, D., Mannani, I., 2017. Bulk-carbonate and belemnite carbon-isotope records across the Pliensbachian-Toarcian boundary on the northern margin of Gondwana (Issouka, Middle Atlas, Morocco). *Palaeogeogr. Palaeoclimatol. Palaeoecol.* 466, 128–136.
- Ait-Itto, F.Z., Martinez, M., Price, G.D., Addi, A.A., 2018. Synchronization of the astronomical time scales in the Early Toarcian: a link between anoxia, carbon-cycle perturbation, mass extinction and volcanism. *Earth Planet. Sci. Lett.* 493, 1–11.
- Al-Suwaidi, A.H., Hesselbo, S.P., Damborenea, S.E., Manceño, M.O., Jenkyns, H.C., Riccardi, A.C., Angelozzi, G.N., Baudin, F., 2016. The Toarcian Oceanic Anoxic Event (Early Jurassic) in the Neuquén Basin, Argentina: a reassessment of age and carbon isotope stratigraphy. *J. Geol.* 124 (2), 171–193.
- Arabas, A., Schlögl, J., Meister, C., 2017. Early Jurassic carbon and oxygen isotope records and seawater temperature variations: insights from marine carbonate and belemnite rostra (Pieniny Klippen Belt, Carpathians). *Palaeogeogr. Palaeoclimatol. Palaeoecol.* 485, 119–135.
- Baeza-Carratalá, J.F., 2013. Diversity patterns of Early Jurassic brachiopod assemblages from the westernmost Tethys (Eastern Subbetic). *Palaeogeogr. Palaeoclimatol. Palaeoecol.* 381, 76–91.
- Baeza-Carratalá, J.F., Garcia-Joral, F., Giannetti, A., Tent-Manclús, J.E., 2015. Evolution of the last koninckinids (Athyridida, Koninckinidae), a precursor signal of the Early Toarcian mass extinction event in the Western Tethys. *Palaeogeogr. Palaeoclimatol. Palaeoecol.* 429, 41–56.
- Baeza-Carratalá, J.F., Reolid, M., Garcia-Joral, F., 2017. New deep-water brachiopod resilient assemblage from the South-Iberian Palaeomargin (Western Tethys) and its significance for the brachiopod adaptive strategies around the Early Toarcian Mass Extinction Event. *Bull. Geosci.* 92, 233–256.
- Bailey, T.R., Rosenthal, Y., McArthur, J.M., Van de Schootbrugge, B., Thirlwall, M.F., 2003. Paleoclimatographic changes of the late Pliensbachian–Early Toarcian interval: a possible link to the genesis of an Oceanic Anoxic Event. *Earth Planet. Sci. Lett.* 212 (3–4), 307–320.
- Beaufort, L., 1991. Adaptation of the random settling method for quantitative studies of calcareous nannofossils. *Micropaleontology* 37, 415–418.
- Bodin, S., Mattioli, E., Fröhlich, S., Marshall, J.D., Boutin, L., Lahsini, S., Redfern, J., 2010. Toarcian carbon isotope shifts and nutrient changes from the Northern margin of Gondwana (High Atlas, Morocco, Jurassic): palaeoenvironmental implications. *Palaeogeogr. Palaeoclimatol. Palaeoecol.* 297 (2), 377–390.
- Bodin, S., Krencker, F.N., Kothe, T., Hoffmann, R., Mattioli, E., Heimhofer, U., Kabiri, L., 2016. Perturbation of the carbon cycle during the late Pliensbachian–early Toarcian: new insight from high-resolution carbon isotope records in Morocco. *J. Afr. Earth Sci.* 116, 89–104.
- Boullila, S., Hinnov, L.A., 2017. A review of tempo and scale of the early Jurassic Toarcian OAE: implications for carbon cycle and sea level variations. *Newsl. Stratigr.* 50 (4), 363–389.
- Boullila, S., Galbrun, B., Huret, E., Hinnov, L.A., Rouget, I., Gardin, S., Bartolini, A., 2014. Astronomical calibration of the Toarcian Stage: implications for sequence stratigraphy and duration of the early Toarcian OAE. *Earth Planet. Sci. Lett.* 386, 98–111.
- Boullila, S., Galbrun, B., Sadki, D., Gardin, S., Bartolini, A., 2019. Constraints on the duration of the early Toarcian T-OAE and evidence for carbon-reservoir change from the High Atlas (Morocco). *Glob. Planet. Chang.* 175, 113–128.
- Bown, P., 1998. *Calcareous Nannofossil Biostratigraphy*. Chapman and Hall; Kluwer Academic, pp. 1–315.
- Brame, H.M.R., Martindale, R.C., Ettinger, N.P., Debeljak, I., Vasseur, R., Lathuilière, B., Kabiri, L., Bodin, S., 2019. Stratigraphic distribution and paleoecological significance of Early Jurassic (Pliensbachian-Toarcian) lithotid-coral reefal deposits from the Central High Atlas of Morocco. *Palaeogeogr. Palaeoclimatol. Palaeoecol.* 514, 813–837.
- Bucefalo-Palliani, R., Mattioli, E., Riding, J., 2002. The response of marine phytoplankton and sedimentary organic matter to the early Toarcian (Lower Jurassic) oceanic anoxic event in northern England. *Mar. Micropaleontol.* 46, 223–245.
- Caruthers, A.H., Smith, P.L., Gröcke, D.R., 2013. The Pliensbachian–Toarcian (Early Jurassic) extinction, a global multi-phased event. *Palaeogeogr. Palaeoclimatol. Palaeoecol.* 386, 104–118.
- Caswell, B.A., Coe, A.L., 2012. A high-resolution shallow marine record of the Toarcian (Early Jurassic) Oceanic Anoxic Event from the East Midlands Shelf, UK. *Palaeogeogr. Palaeoclimatol. Palaeoecol.* 365, 124–135.
- Caswell, B.A., Dawn, S.J., 2019. Recovery of benthic communities following the Toarcian oceanic anoxic event in the Cleveland Basin, UK. *Palaeogeogr. Palaeoclimatol. Palaeoecol.* 521, 114–126.
- Caswell, B.A., Frid, C.L., 2017. Marine ecosystem resilience during extreme deoxygenation: the Early Jurassic oceanic anoxic event. *Oecologia* 183, 275–290.
- Caswell, B.A., Coe, A.L., Cohen, A.S., 2009. New range data for marine invertebrate species across the early Toarcian (Early Jurassic) mass extinction. *J. Geol. Soc.* 166 (5), 859–872.
- Danise, S., Twitchett, R.J., Little, C.T.S., 2015. Environmental controls on Jurassic marine ecosystems during global warming. *Geology* 43, 263–266.
- Danise, S., Clémence, M.E., Price, G.D., Murphy, D.P., Gómez, J.J., Twitchett, R.J., 2019. Stratigraphic and environmental control on marine benthic community change through the early Toarcian extinction event (Iberian Range, Spain). *Palaeogeogr. Palaeoclimatol. Palaeoecol.* 524, 183–200.
- Dera, G., Pellenard, P., Neige, P., Deconinck, J.F., Pucéat, E., Dommergues, J.L., 2009. Distribution of clay minerals in Early Jurassic Peritethyan seas: palaeoclimatic

- significance inferred from multiproxy comparisons. *Palaeogeogr. Palaeoclimatol. Palaeoecol.* 271 (1–2), 39–51.
- Dunhill, A.M., Foster, W.J., Azale, S., Sciberras, J., Twitchett, R.J., 2018. Modelling determinants of extinction across two Mesozoic hyperthermal events. *Proc. R. Soc. B* 285 (1889) p.20180404.
- Elmi, S., Rulleau, L., Gabilly, J., Mouterde, R., 1997. Toarcien (coord.). In: Cariou, E., Hantzpergue, P. (Eds.), *Biostratigraphie du Jurassique ouest-européen et méditerranéen: zonations parallèles et distribution des invertébrés et microfossiles*, Vol. 17. Bulletin du Centre de Recherches Elf Exploration Production, Mémoires, pp. 25–40.
- Ettinger, N.P., Larson, T.E., Kerans, C., Thibodeau, A.M., Hattori, K.E., Kacur, S.M., Martindale, R.C., 2020. Ocean acidification and photic-zone anoxia at the Toarcian Oceanic Anoxic Event: insights from the Adriatic Carbonate Platform. *Sedimentology*. <https://doi.org/10.1111/sed.12786>.
- Fantasia, A., Föllmi, K.B., Adatte, T., Spangenberg, J.E., Mattioli, E., 2019. Expression of the toarcian oceanic anoxic event: new insights from a swiss transect. *Sedimentology* 66 (1), 262–284.
- Ferreira, J., Mattioli, E., Sucherás-Marx, B., Giraud, F., Duarte, L.V., Pittet, B., Suan, G., Hassler, A., Spangenberg, J.E., 2019. Western Tethys Early and Middle Jurassic calcareous nannofossil biostratigraphy. *Earth Sci. Rev.* <https://doi.org/10.1016/j.earscirev.2019.102908>.
- Gahr, M.E., 2005. Response of Lower Toarcian (Lower Jurassic) macrobenthos of the Iberian Peninsula to sea level changes and mass extinction. *J. Iber. Geol.* 31 (2), 197–215.
- Gallego-Torres, D., Reolid, M., Nieto-Moreno, V., Martínez-Casado, F.J., 2015. Pyrite framboid size distribution as a record for relative variations in sedimentation rate: an example on the Toarcian Oceanic Anoxic Event in Southiberian Palaeomargin. *Sediment. Geol.* 330 (5), 9–73.
- García-Joral, F., Goy, A., 2009. Toarcian (Lower Jurassic) brachiopods in Asturias (Northern Spain): stratigraphic distribution, critical events and palaeobiogeography. *Geobios* 42, 255–264.
- García-Joral, F., Gómez, J.J., Goy, A., 2011. Mass extinction and recovery of the Early Toarcian (Early Jurassic) brachiopods linked to climate change in northern and Central Spain. *Palaeogeogr. Palaeoclimatol. Palaeoecol.* 302, 367–380.
- Gaździcki, A., Michalík, J., Planderová, E., Sýkora, M., 1979. An Upper Triassic–Lower Jurassic sequence in the Krížna nappe (West Tatra Mountains, West Carpathians, Czechoslovakia). *Západ. Karp. Geol.* 5, 119–148.
- Geisen, M., Bollmann, J., Herrle, J.O., Mutterlose, J., Young, J.R., 1999. Calibration of the random settling technique for calculation of absolute abundances of calcareous nannoplankton. *Micropaleontology* 45 (4), 437–442.
- Gómez, J.J., Goy, A., 2011. Warming-driven mass extinction in the Early Toarcian (Early Jurassic) of northern and Central Spain. Correlation with other time-equivalent European sections. *Palaeogeogr. Palaeoclimatol. Palaeoecol.* 306 (3–4), 176–195.
- Gómez, J.J., Goy, A., Canales, M.L., 2008. Seawater temperature and carbon isotope variations in belemnites linked to mass extinction during the Toarcian (Early Jurassic) in Central and Northern Spain. Comparison with other European sections. *Palaeogeogr. Palaeoclimatol. Palaeoecol.* 258 (1–2), 28–58.
- Gradziński, M., Tyszká, J., Uchman, A., Jach, R., 2004. Large microbial-foraminiferal ooids from condensed Lower–Middle Jurassic deposits: a case study from the Tatra Mountains, Poland. *Palaeogeogr. Palaeoclimatol. Palaeoecol.* 213 (1–2), 133–151.
- Gröcke, D.R., Hori, R.S., Trabucho-Alexandre, J., Kemp, D.B., Schwark, L., 2011. An open ocean record of the Toarcian oceanic anoxic event. *Solid Earth* 2 (2), 245–257.
- Haas, J., 2012. Influence of global, regional, and local factors on the genesis of the Jurassic manganese ore formation in the Transdanubian Range, Hungary. *Ore Geol. Rev.* 47, 77–86.
- Hardenbol, J., Thierry, J., Farley, M.B., de Graciansky, P.-C., Vail, P.R., 1998. Mesozoic and Cenozoic sequence chronostratigraphic framework of European basins. In: de Graciansky, P.-C., Hardenbol, J., Jacquin, T., Vail, P.R. (Eds.), *Mesozoic and Cenozoic Sequence Stratigraphy of European Basins*, Vol. 60. SEPM, Special Publications, pp. 3–13.
- Harries, P.J., Little, C.T., 1999. The early Toarcian (Early Jurassic) and the Cenomanian–Turonian (Late Cretaceous) mass extinctions: similarities and contrasts. *Palaeogeogr. Palaeoclimatol. Palaeoecol.* 154 (1–2), 39–66.
- Häusler, H., Plašienka, D., Polák, M., 1993. Comparison of Mesozoic successions in the Central Eastern Alps and the Central Western Carpathians. *Jahrb. Geol. Bundesanst.* 136, 715–739.
- Hermoso, M., Pellenard, P., 2014. Continental weathering and climatic changes inferred from clay mineralogy and paired carbon isotopes across the early to middle Toarcian in the Paris Basin. *Palaeogeogr. Palaeoclimatol. Palaeoecol.* 399, 385–393.
- Hermoso, M., Le Callonnec, L., Minoletti, F., Renard, M., Hesselbo, S.P., 2009. Expression of the Early Toarcian negative carbon-isotope excursion in separated carbonate microfossils (Jurassic, Paris Basin). *Earth Planet. Sci. Lett.* 277 (1–2), 194–203.
- Hermoso, M., Minoletti, F., Rickaby, R.E., Hesselbo, S.P., Baudin, F., Jenkyns, H.C., 2012. Dynamics of a stepped carbon-isotope excursion: ultra high-resolution study of Early Toarcian environmental change. *Earth Planet. Sci. Lett.* 319, 45–54.
- Hermoso, M., Minoletti, F., Pellenard, P., 2013. Black shale deposition during Toarcian super-greenhouse driven by sea level. *Clim. Past* 9, 2703–2712.
- Hesselbo, S.P., Pieńkowski, G., 2011. Stepwise atmospheric carbon-isotope excursion during the Toarcian oceanic anoxic event (Early Jurassic, Polish Basin). *Earth Planet. Sci. Lett.* 301 (1–2), 365–372.
- Hesselbo, S.P., Jenkyns, H.C., Duarte, L.V., Oliveira, L.C., 2007. Carbon-isotope record of the Early Jurassic (Toarcian) Oceanic Anoxic Event from fossil wood and marine carbonate (Lusitanian Basin, Portugal). *Earth Planet. Sci. Lett.* 253 (3–4), 455–470.
- Howarth, M.K., 1992a. The ammonite family Hildoceratidae in the Lower Jurassic of Britain. Part 1. *Monogr. Palaeontol. Soc.* 145, 1–106.
- Howarth, M.K., 1992b. The ammonite family Hildoceratidae in the Lower Jurassic of Britain. Part 2. *Monogr. Palaeontol. Soc.* 146, 107–200.
- Huang, C., Hesselbo, S.P., 2014. Pacing of the Toarcian Oceanic Anoxic Event (Early Jurassic) from astronomical correlation of marine sections. *Gondwana Res.* 25 (4), 1348–1356.
- Iwańczuk, J., Iwanow, A., Wierzbowski, A., 2013. Lower Jurassic to lower Middle Jurassic succession at Kopy Sołtysa and Placziwa Skala in the eastern Tatra Mts (Western Carpathians) of Poland and Slovakia: stratigraphy, facies and ammonites. *Vol. Jurassica* 11 (11), 19–58.
- Izumi, K., Kemp, D.B., Itamiya, S., Inui, M., 2018. Sedimentary evidence for enhanced hydrological cycling in response to rapid carbon release during the early Toarcian oceanic anoxic event. *Earth Planet. Sci. Lett.* 481, 162–170.
- Jach, R., 2002. Lower Jurassic spiculite series from the Krížna Unit in the Western Tatra Mts, Western Carpathians, Poland. *Ann. Soc. Geol. Pol.* 72, 131–144.
- Jach, R., 2005. Storm-dominated deposition of the Lower Jurassic crinoidal limestones in the Krížna unit, Western Tatra Mountains, Poland. *Facies* 50, 561–572.
- Jenkyns, H., 1988. The early Toarcian (Jurassic) anoxic event–stratigraphic, sedimentary, and geochemical evidence. *Am. J. Sci.* 288 (2), 101–151.
- Jenkyns, H., Clayton, C.J., 1997. Lower Jurassic epicontinental carbonates and mudstones from England and Wales: chemostratigraphic signals and the early Toarcian anoxic event. *Sedimentology* 44 (4), 687–706.
- Jenkyns, H.C., Géczy, B., Marshall, J.D., 1991. Jurassic manganese carbonates of Central Europe and the early Toarcian anoxic event. *J. Geol.* 99 (2), 137–149.
- Jenkyns, H.C., Jones, C.E., Gröcke, D.R., Hesselbo, S.P., Parkinson, D.N., 2002. Chemostratigraphy of the Jurassic System: applications, limitations and implications for palaeoceanography. *J. Geol. Soc.* 159 (4), 351–378.
- Jiménez, A.P., Jimenez de Cisneros, C., Rivas, P., Vera, J.A., 1996. The early Toarcian anoxic event in the westernmost Tethys (Subbetic). *Palaeogeographic and paleobiogeographic significance*. *J. Geol.* 104, 399–416.
- Kemp, D.B., Coe, A.L., Cohen, A.S., Schwark, L., 2005. Astronomical pacing of methane release in the Early Jurassic period. *Nature* 437 (7057) p.396.
- Koša, E., 1998. Lithostratigraphy and depositional environment of Lower–Middle Jurassic crinoidal limestone formations of the Vysoká Nappe Unit (Malé Karpaty Mts., Western Carpathians). *Geol. Carpath.* 49, 329–340.
- Kraimer, K., Mostler, H., 1997. Die Lias-Beckenentwicklung der Unkenker Synklinale (Nördliche Kalkalpen, Salzburg) unter besonderer Berücksichtigung der Scheibenberg Formation. *Geol. Paläontol. Mitt. Innsbruck* 22, 1–41.
- Kraimer, K., Mostler, H., Haditsch, J.G., 1994. Jurassische Beckenbildung in den Nördlichen Kalkalpen bei Lofer (Salzburg) unter besonderer Berücksichtigung der Manganerz-Genese. *Abh. Geol. Bundesanst.* 50, 257–293.
- Krencker, F.N., Fantasia, A., Danisch, J., Martindale, R., Kabiri, L., El Ouali, M., Bodin, S., 2020. Two-phased collapse of the shallow-water carbonate factory during the late Pliensbachian–Toarcian driven by changing climate and enhanced continental weathering in the Northwestern Gondwana Margin. *Earth Sci. Rev.* 208, 103254.
- Lefeld, J., Gaździcki, A., Iwanow, A., Krajewski, K., Wójcik, K., 1985. Jurassic and Cretaceous lithostratigraphic units in the Tatra Mts. *Stud. Geol. Pol.* 84, 7–93.
- Léonide, P., Floquet, M., Duret, C., Baudin, F., Pittet, B., Lécuyer, C., 2012. Drowning of a carbonate platform as a precursor stage of the Early Toarcian global anoxic event (Southern Provence sub-Basin, South-east France). *Sedimentology* 59 (1), 156–184.
- Littler, K., Hesselbo, S.P., Jenkyns, H.C., 2010. A carbon-isotope perturbation at the Pliensbachian–Toarcian boundary: evidence from the Lias Group, NE England. *Geol. Mag.* 147 (2), 181–192.
- Macchioni, F., Cecca, F., 2002. Biodiversity and biogeography of middle–late Liassic ammonoids: implications for the early Toarcian mass extinction. *Geobios* 35, 165–175.
- Marshall, J.D., 1992. Climatic and oceanographic isotopic signals from the carbonate rock record and their preservation. *Geol. Mag.* 129 (2), 143–160.
- Martindale, R.C., Aberhan, M., 2017. Response of macrobenthic communities to the Toarcian Oceanic Anoxic Event in northeastern Panthalassa (Ya Ha Tinda, Alberta, Canada). *Palaeogeogr. Palaeoclimatol. Palaeoecol.* 478, 103–120.
- Mattioli, E., Erba, E., 1999. Biostratigraphic synthesis of calcareous nannofossil events in the Tethyan Jurassic. *Riv. Ital. Paleontol. Stratigr.* 105 (3), 343–376.
- Mattioli, E., Pittet, B., Petitpierre, L., Mailliot, S., 2009. Dramatic decrease of pelagic carbonate production by nannoplankton across the Early Toarcian anoxic event (T-OAE). *Glob. Planet. Chang.* 65 (3–4), 134–145.
- McArthur, J.M., Algeo, T.J., Van de Schootbrugge, B., Li, Q., Howarth, R.J., 2008. Basinal restriction, black shales, Re-Os dating, and the Early Toarcian (Jurassic) oceanic anoxic event. *Paleoceanography* 23 (4).
- McCrea, J.M., 1950. On the isotopic chemistry of carbonates and a paleotemperature scale. *J. Chem. Phys.* 18 (6), 849–857.
- McElwain, J.C., Wade-Murphy, J., Hesselbo, S.P., 2005. Changes in carbon dioxide during an oceanic anoxic event linked to intrusion into Gondwana coals. *Nature* 435 (7041) p.479.
- Menini, A., Mattioli, E., Spangenberg, J.E., Pittet, B., Suan, G., 2019. New calcareous nannofossil and carbon isotope data for the Pliensbachian/Toarcian boundary (Early Jurassic) in the western Tethys and their paleoenvironmental implications. *NewsL. Stratigr.* 52 (173–196), 2019. <https://doi.org/10.1127/nos/2018/0476>.
- Míguez-Salas, O., Rodríguez-Tovar, F.J., Duarte, L.V., 2017. Selective incidence of the toarcian oceanic anoxic event on macroinvertebrate marine communities: a case from the Lusitanian basin, Portugal. *Lethaia* 50 (4), 548–560.
- Mišík, M., Rakús, M., 1964. Bemerkungen zu räumlichen Beziehungen des Lias und zur Paläogeographie des Mesozoikum in der Grossen Fatra. *Zborník Geol. Vied Západ. Karp.* 1, 159–199.
- Montero-Serrano, J.C., Föllmi, K.B., Adatte, T., Spangenberg, J.E., Tribouillard, N., Fantasia, A., Suan, G., 2015. Continental weathering and redox conditions during the early Toarcian Oceanic Anoxic Event in the northwestern Tethys: insight from the

- Posidonia Shale section in the Swiss Jura Mountains. *Palaeogeogr. Palaeoclimatol. Palaeoecol.* 429, 83–99.
- Müller, T., Price, G.D., Bajnai, D., Nyerges, A., Kesjár, D., Raucsik, B., Varga, A., Judik, K., Fekete, J., May, Z., Pálffy, J., 2017. New multiproxy record of the Jenkyns Event (also known as the Toarcian Oceanic Anoxic Event) from the Mecsek Mountains (Hungary): differences, duration and drivers. *Sedimentology* 64 (1), 66–86.
- Müller, T., Jurikova, H., Gutjahr, M., Tomašových, A., Schlögl, J., Liebetrau, V., Milovský, R., Suan, G., Mattioli, E., Pittet, B., Eisenhauer, A., 2020. Ocean acidification during the early Toarcian extinction event: Evidence from boron isotopes in brachiopods. *Geology*. <https://doi.org/10.1130/G47781.1>, 48.
- Neumeister, S., Gratzner, R., Algeo, T.J., Bechtel, A., Gawlick, H.J., Newton, R.J., Sachsenhofer, R.F., 2015. Oceanic response to Pliensbachian and Toarcian magmatic events: Implications from an organic-rich basinal succession in the NW Tethys. *Glob. Planet. Chang.* 126, 62–83.
- Pálffy, J., Smith, P.L., 2000. Synchrony between Early Jurassic extinction, oceanic anoxic event, and the Karoo-Ferrar flood basalt volcanism. *Geology* 28 (8), 747–750.
- Perilli, N., 2000. Calibration of early–middle Toarcian nannofossil events based on high-resolution ammonite biostratigraphy in two expanded sections from the Iberian Range (East Spain). *Mar. Micropaleontol.* 39 (1–4), 293–308.
- Piazza, V., Duarte, L.V., Renaudie, J., Aberhan, M., 2019. Reductions in body size of benthic macroinvertebrates as a precursor of the early Toarcian (Early Jurassic) extinction event in the Lusitanian Basin, Portugal. *Paleobiology* 45, 296–316.
- Pittet, B., Suan, G., Lenoir, F., Duarte, L.V., Mattioli, E., 2014. Carbon isotope evidence for sedimentary discontinuities in the lower Toarcian of the Lusitanian Basin (Portugal): sea level change at the onset of the Oceanic Anoxic Event. *Sediment. Geol.* 303, 1–14.
- Polgári, M., Hein, J.R., Bíró, L., Gyollai, I., Németh, T., Sajgó, C., Fekete, J., Schwark, L., Pál-Molnár, E., Hámor-Vidó, M., Vigh, T., 2016. Mineral and chemostratigraphy of a Toarcian black shale hosting Mn-carbonate microbialites (Úrkút, Hungary). *Palaeogeogr. Palaeoclimatol. Palaeoecol.* 459, 99–120.
- Rakús, M., 1963. Distribution of the Toarcian lithofacies in the central zone of the West Carpathians. *Geol. Sbor. Slov. Akad. Vied* 14, 19–27.
- Rakús, M., 1964. Paläontologische studien im Lias der Grossen Fatra und Westteils der Niederen Tatra. In: *Sbor. Geol. Vied, Západ Karpaty*, pp. 94–154.
- Rakús, M., 1984. Skladaná skala – quarry. Guide to geological excursion in the West Carpathians Mts. Guide to geological excursion. In: IGCP Project No. 198. The Evolution of the Northern Margin of Tethys. *Geol. Ústav Dionýza Stúra, Bratislava*, pp. 1–99.
- Reolid, J., Reolid, M., 2020. Geochemical compositional mapping of Lower Jurassic trace fossils: palaeoenvironmental significance and methodological implications. *Palaeogeogr. Palaeoclimatol. Palaeoecol.* 538, 109456.
- Reolid, M., Rodríguez-Tovar, F.J., Marok, A., Sebane, A., 2012a. The Toarcian oceanic anoxic event in the Western Saharan Atlas, Algeria (North African paleomargin): role of anoxia and productivity. *Geol. Soc. Am. Bull.* 124, 1646–1664.
- Reolid, M., Sebane, A., Rodríguez-Tovar, F.J., Marok, A., 2012b. Foraminiferal morphogroups as a tool to approach the Toarcian Anoxic Event in the Western Saharan Atlas (Algeria). *Palaeogeogr. Palaeoclimatol. Palaeoecol.* 323, 87–99.
- Reolid, M., Emanuela, M., Nieto, L.M., Rodríguez-Tovar, F.J., 2014. The Early Toarcian oceanic anoxic event in the External Subbetic (Southiberian Paleomargin, Westernmost Tethys): geochemistry, nannofossils and ichnology. *Palaeogeogr. Palaeoclimatol. Palaeoecol.* 411, 79–94.
- Rita, P., Nätscher, P., Duarte, L.V., Weis, R., De Baets, K., 2019. Mechanisms and drivers of belemnite body-size dynamics across the Pliensbachian–Toarcian crisis. *R. Soc. Open Sci.* 6, 190494.
- Rodríguez-Tovar, F.J., Reolid, M., 2013. Environmental conditions during the Toarcian Oceanic Anoxic Event (T-OAE) in the westernmost Tethys: influence of the regional context on a global phenomenon. *Bull. Geosci.* 88 (4), 697–712.
- Rodríguez-Tovar, F.J., Uchman, A., 2010. Ichnofabric evidence for the lack of bottom anoxia during the Lower Toarcian oceanic anoxic event in the Fuente de la Vidriera section, Betic Cordillera, Spain. *Palaios* 25 (9), 576–587.
- Röhl, H.J., Schmid-Röhl, A., Oschmann, W., Frimmel, A., Schwark, L., 2001. The Posidonia Shale (Lower Toarcian) of SW-Germany: an oxygen-depleted ecosystem controlled by sea level and palaeoclimate. *Palaeogeogr. Palaeoclimatol. Palaeoecol.* 165 (1–2), 27–52.
- Ros-Franch, S., Echevarría, J., Damborenea, S.E., Mancenido, M.O., Jenkyns, H.C., Al-Suwaidi, A., Hesselbo, S.P., Riccardi, A.C., 2019. Population response during an Oceanic Anoxic Event: the case of Posidonotis (Bivalvia) from the lower Jurassic of the Neuquén Basin, Argentina. *Palaeogeogr. Palaeoclimatol. Palaeoecol.* 525, 57–67.
- Ruesam, W., Müller, T., Kovács, J., Pálffy, J., Schwark, L., 2018. Environmental response to the early Toarcian carbon cycle and climate perturbations in the northeastern part of the West Tethys shelf. *Gondwana Res.* 59, 144–158.
- Ruesam, W., Mayer, B., Schwark, L., 2019. Cryosphere carbon dynamics control early Toarcian global warming and sea level evolution. *Glob. Planet. Chang.* 172, 440–453.
- Sabatino, N., Neri, R., Bellanca, A., Jenkyns, H.C., Baudin, F., Parisi, G., Masetti, D., 2009. Carbon-isotope records of the Early Jurassic (Toarcian) oceanic anoxic event from the Valdorbia (Umbria–Marche Apennines) and Monte Mangart (Julian Alps) sections: Palaeoceanographic and stratigraphic implications. *Sedimentology* 56 (5), 1307–1328.
- Šimo, V., Tomašových, A., 2013. Trace-fossil assemblages with a new ichnogenus in “spotted” (Fleckenmergel–Fleckenkalk) deposits: a signature of oxygen-limited benthic communities. *Geol. Carpath.* 64 (5), 355–374.
- Smith, A.B., Stockley, B., 2005. The geological history of deep-sea colonization by echinoids: roles of surface productivity and deep-water ventilation. *Proc. R. Soc. B Biol. Sci.* 272 (1565), 865–869.
- Suan, G., Mattioli, E., Pittet, B., Mailliot, S., Lécuyer, C., 2008a. Evidence for major environmental perturbation prior to and during the Toarcian (Early Jurassic) oceanic anoxic event from the Lusitanian Basin, Portugal. *Paleoceanography* 23 (1), PA1202.
- Suan, G., Pittet, B., Bour, I., Mattioli, E., Duarte, L.V., Mailliot, S., 2008b. Duration of the Early Toarcian carbon isotope excursion deduced from spectral analysis: consequence for its possible causes. *Earth Planet. Sci. Lett.* 267 (3–4), 666–679.
- Suan, G., Mattioli, E., Pittet, B., Lécuyer, C., Suchéras-Marx, B., Duarte, L.V., Philippe, M., Reggiani, L., Martineau, F., 2010. Secular environmental precursors to Early Toarcian (Jurassic) extreme climate changes. *Earth Planet. Sci. Lett.* 290 (3–4), 448–458.
- Suan, G., Van De Schootbrugge, B., Adatte, T., Fiebig, J., Oschmann, W., 2015. Calibrating the magnitude of the Toarcian carbon cycle perturbation. *Paleoceanography* 30 (5), 495–509.
- Suan, G., Schlögl, J., Mattioli, E., 2016. Bio-and chemostratigraphy of the Toarcian organic-rich deposits of some key successions of the Alpine Tethys. *Newsl. Stratigr.* 49 (3), 401–419.
- Suan, G., Schöllhorn, I., Schlögl, J., Segit, T., Mattioli, E., Lécuyer, C., Fourel, F., 2018. Euxinic conditions and high sulfur burial near the European shelf margin (Pieniny Klippen Belt, Slovakia) during the Toarcian oceanic anoxic event. *Glob. Planet. Chang.* 170, 246–259.
- Svensen, H., Planke, S., Chevillier, L., Malthes-Sørensen, A., Corfu, F., Jamveit, B., 2007. Hydrothermal venting of greenhouse gases triggering Early Jurassic global warming. *Earth Planet. Sci. Lett.* 256 (3–4), 554–566.
- Them, T.R., Gill, B.C., Caruthers, A.H., Gerhardt, A.M., Gröcke, D.R., Lyons, T.W., Marroquin, S.M., Nielsen, S.G., Alexandre, J.P.T., Owens, J.D., 2018. Thallium isotopes reveal protracted anoxia during the Toarcian (Early Jurassic) associated with volcanism, carbon burial, and mass extinction. *Proc. Natl. Acad. Sci.* 115 (26), 6596–6601.
- Thibault, N., Ruhl, M., Ullmann, C.V., Korte, C., Kemp, D.B., Gröcke, D.R., Hesselbo, S.P., 2018. The wider context of the Lower Jurassic Toarcian oceanic anoxic event in Yorkshire coastal outcrops, UK. *Proc. Geol. Assoc.* 129 (3), 372–391.
- Thierry, J., 2000. Late Toarcian. In: Dercourt, J., Gaetani, M., Vrielynck, B., Barrier, E., Biju-Duval, B., Brunet, M.F., Cadet, J.P., Crasquin, S., Sandulescu, M. (Eds.), *Atlas Peri-Tethys*. Palaeogeographical Maps.
- Thuy, B., Gale, A.S., Kroh, A., Kucera, M., Numberger-Thuy, L.D., Reich, M., Stöhr, S., 2012. Ancient origin of the modern deep-sea fauna. *PLoS One* 7 (10), e46913.
- Trecalli, A., Spangenberg, J., Adatte, T., Föllmi, K.B., Parente, M., 2012. Carbonate platform evidence of ocean acidification at the onset of the early Toarcian oceanic anoxic event. *Earth Planet. Sci. Lett.* 357, 214–225.
- Ullmann, C.V., Boyle, R., Duarte, L.V., Hesselbo, S.P., Kasemann, S.A., Klein, T., Lenton, T.M., Piazza, V., Aberhan, M., 2020. Warm afterglow from the toarcian oceanic Anoxic event drives the success of deep-adapted brachiopods. *Sci. Rep.* 10, 6549.
- van de Schootbrugge, B., Bachan, A., Suan, G., Richo, S., Payne, J.L., 2013. Microbes, mud and methane: cause and consequence of recurrent Early Jurassic anoxia following the end-Triassic mass extinction. *Palaeontology* 56 (4), 685–709.
- Vetö, I., Demény, A., Hertelendi, E., Hetényi, M., 1997. Estimation of primary productivity in the Toarcian Tethys—a novel approach based on TOC, reduced Sulphur and manganese contents. *Palaeogeogr. Palaeoclimatol. Palaeoecol.* 132 (1–4), 355–371.
- Vörös, A., 2005. The smooth brachiopods of the Mediterranean Jurassic: refugees or invaders? *Palaeogeogr. Palaeoclimatol. Palaeoecol.* 223 (3–4), 222–242.
- Wignall, P.B., Newton, R.J., Little, C.T., 2005. The timing of paleoenvironmental change and cause-and-effect relationships during the Early Jurassic mass extinction in Europe. *Am. J. Sci.* 305 (10), 1014–1032.
- Woodfine, R.G., Jenkyns, H.C., Sarti, M., Baroncini, F., Violante, C., 2008. The response of two Tethyan carbonate platforms to the early Toarcian (Jurassic) oceanic anoxic event: environmental change and differential subsidence. *Sedimentology* 55 (4), 1011–1028.
- Xu, W., Ruhl, M., Jenkyns, H.C., Hesselbo, S.P., Riding, J.B., Selby, D., Naafs, B.D.A., Weijers, J.W., Pancost, R.D., Tegelaar, E.W., Idiz, E.F., 2017. Carbon sequestration in an expanded lake system during the Toarcian oceanic anoxic event. *Nat. Geosci.* 10 (2), 129–134.
- Xu, W., Ruhl, M., Jenkyns, H.C., Leng, M.J., Huggett, J.M., Minisini, D., Ullmann, C.V., Riding, J.B., Weijers, J.W., Storm, M.S., Percival, L.M., 2018. Evolution of the Toarcian (Early Jurassic) carbon-cycle and global climatic controls on local sedimentary processes (Cardigan Bay Basin, UK). *Earth Planet. Sci. Lett.* 484, 396–411.